Effects of wood on debris flow runout in small mountain watersheds

Stephen T. Lancaster and Shannon K. Hayes

Department of Geosciences, Oregon State University, Corvallis, Oregon, USA

Gordon E. Grant

USDA Forest Service, Pacific Northwest Research Station, Corvallis, Oregon, USA

[1] Debris flows have typically been viewed as two-phase mixtures of sediment and water, but in forested mountain landscapes, wood can represent a sizable fraction of total flow volume. The effects of this third phase on flow behavior are poorly understood. To evaluate whether wood can have a significant effect on debris flow runout in small mountainous watersheds, we used a landscape-scale model combining empirical, stochastic, and physical submodels of storms, fires, forest growth, tree fall, wood decay, soil production and diffusion, landslide initiation, debris flow runout, and fluvial sediment transport. We examined changes in the cumulative distribution function of debris flow runout lengths in a small (2 km^2) watershed in the Oregon Coast Range due to presence or absence of two hypothesized effects of wood: (1) velocity reduction due to entrainment of wood in the runout path and (2) velocity reduction due to changes in flow direction angle. The model was calibrated such that the distribution for simulations including both effects was similar to that measured in the study basin, and amounts of wood in the simulation and the field, both fallen in small valleys and incorporated by debris flows, were comparable. Removal of either effect, or both, significantly shifted runout length distributions to longer lengths. Simulations and field observations indicate that with wood, fluvial transport is a significant source of sediment output, few debris flows reach the outlet, and debris flow deposits are widely distributed throughout the network. Simulations indicate that without wood, basin sediment yield greatly increases, that yield is dominated by longer-runout debris flows, and that debris flow deposits are concentrated in the low-gradient reach near the outlet. *INDEX TERMS:* 1815 Hydrology: Erosion and sedimentation; 1824 Hydrology: Geomorphology (1625); 1803 Hydrology: Anthropogenic effects; 3210 Mathematical Geophysics: Modeling; *KEYWORDS:* geomorphology, landslide, debris flow, natural hazard, woody debris, landscape evolution

1. Introduction

[2] The application of mixture theory to debris flow dynamics has greatly enhanced our understanding and ability to predict the behavior of debris flows as two-phase systems, i.e., sediment and water, especially in controlled, experimental settings [*Iverson*, 1997; *Iverson et al.*, 2000; *Denlinger and Iverson*, 2001; *Iverson and Denlinger*, 2001]. In forested environments, however, debris flows commonly incorporate wood in quantities comparable to the other constituents, and the effect of that wood on debris flow runout is not known.

[3] *Swanson and Lienkaemper* [1978] and *May* [2002] found that wood in debris flow deposits is an important constituent in terms of quantity, and our own observations and measurements, described herein, confirm this finding. Moreover, wood and sediment behave differently. Field observations indicate that the wood constituent is most often concentrated at the front of the deposit as a wood jam that traps the remainder of the deposit [*Hogan et al.*, 1998] (Figure 1). Such jams are often found at large-angle channel and valley bends and tributary junctions [*Benda and Cundy*, 1990], where, according to our own observations, either long logs become wedged in turns with small radii of curvature or debris flows stop upon collision with valley walls. Recent experiments, which we participated in, at the USGS debris flow flume in Oregon have shown that debris flows mobilize wood in their paths by effectively "bulldozing" it and pushing it along at the flow front (Figure 1). These observations suggest that wood might have two major effects on debris flow runout: (1) momentum conservation requires that debris flows must lose velocity to accelerate and entrain wood in their paths and (2) field observations indicate that debris flows with snouts of large wood may lose velocity at turns, unlike debris flows without wood, which move fluidly through bends with little loss of velocity (R.M. Iverson, USGS Cascades Volcano
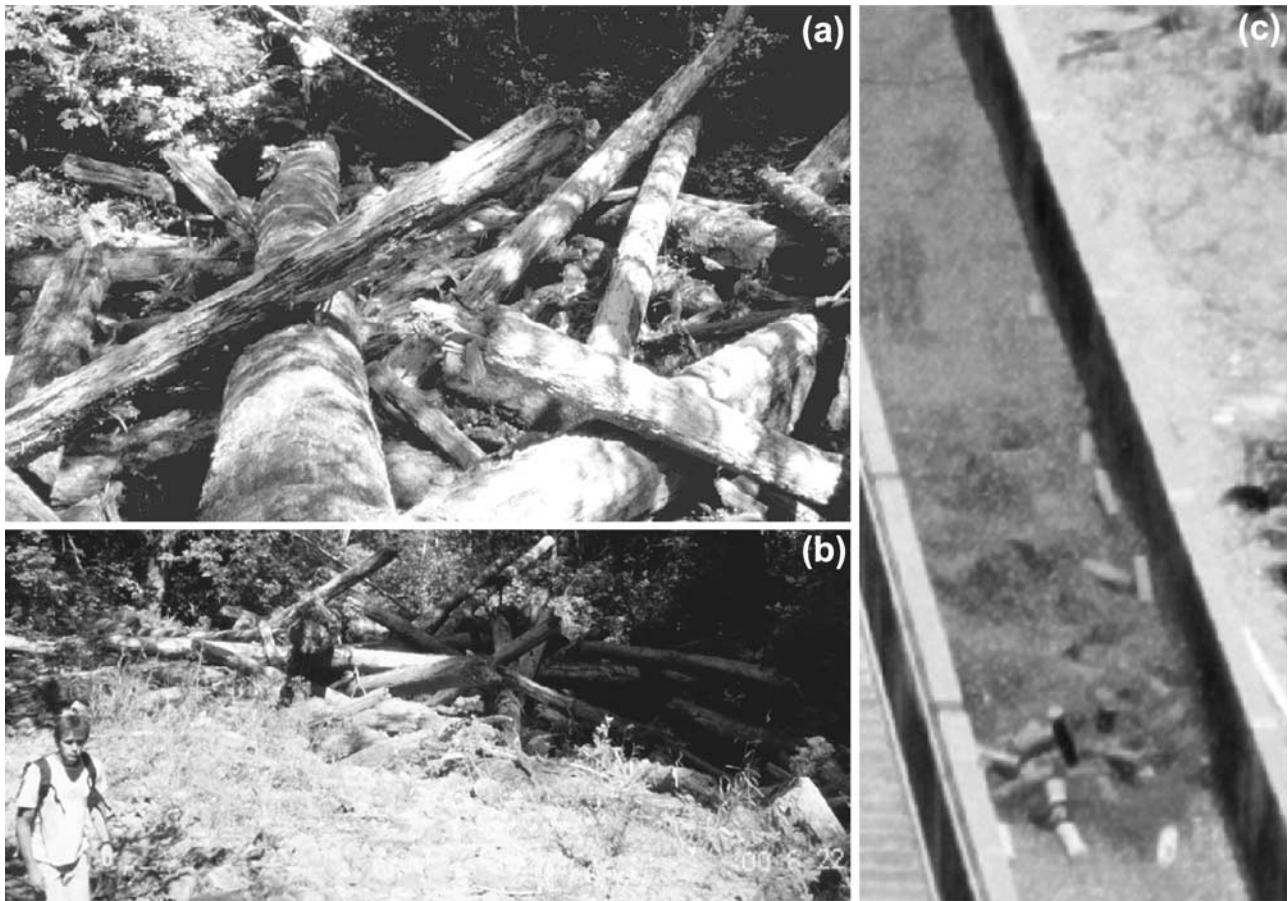
Figure 1. Dam-forming wood jam at the front of a debris flow deposit in the Oregon Coast Range, views (a) downstream from the wood jam and (b) downstream from the sediment dammed behind the wood jam. (c) Woody snout forming at the front of a debris flow in the USGS experimental flume in Oregon, September 1999. Individual logs are 2 ft. (0.61 m) long.

Observatory, personal communication, 2002). Other effects might include resistance to breakage of large, anchored logs in debris flows' paths, resistance to uprooting or breakage of standing trees in debris flows' paths, and resistance to motion of large pieces of wood that dig into the bed and banks and become tangled with one another.

[4] Debris flows from forested mountain watersheds have emerged as an important issue, both as natural hazards and for their impacts on aquatic ecosystems. Policy makers in the Pacific Northwest, for example, wish to assess the effects of forest management practices, both current and proposed, on streams that are spawning habitat for threatened and endangered salmonid fish species. One important way that forest practices can affect aquatic habitat is through the interaction between forests and mass movements. In the Oregon Coast Range, these mass movements are typically shallow, soil layer failures that move downslope and downstream as debris flows. In addition to sediment and water, these debris flows typically contain a large fraction of wood. This wood is more important, e.g., for trapping sediment, forming pools, and, thus enhancing aquatic habitat, where logging has reduced wood input from riparian areas [*Montgomery et al.*, 2003]. In fact, management prescriptions such as extending riparian buffers to the smallest headwater streams are based on debris flows' delivery of wood to fishbearing streams. Such p   ptions have already been

enacted on federal lands in the Pacific Northwest [*Forest Ecosystem Management Assessment Team* (*FEMAT*), 1993], even though the effects of that wood on debris flow runout are poorly understood.

[5] Our goal is to understand whether wood has a significant effect on debris flow runout lengths in small, mountain watersheds. If the effect is significant, how large might it be, and what are its implications for sediment and wood delivery to fish-bearing streams?

[6] In the field it is difficult to quantifiably discern the effects of wood on debris flow runout lengths [*May*, 2002]. We instead turn to modeling, which allows us to perform complex "thought experiments" simulating different effects of wood in the same drainage basin. In real watersheds the interaction of wood with debris flows occurs in the context of many other processes and controls, including hillslope soil production and transport, forest dynamics, landslide initiation, and fluvial sediment transport. To examine the effect of wood in the context of these complex interactions we have developed a physically based model that simulates many events throughout a watershed and routes them through a topographically realistic channel network. The role of the present modeling study, and many others using multiparameter models, is to guide our understanding of process linkages in the landscape rather than to make precise predictions [see, e.g., *Haff*, 1996; *Lancaster and*

Figure 2. Location map of the Oregon Coast Range showing the Hoffman Creek watershed (outlined with dotted line) and study basin (outlined with solid line).

Grant, 2003]. The model is similar to that of *Lancaster et al.* [2001]. A simplified model of debris flow runout incorporated within a landscape evolution model is used to simulate different scenarios in the same small ($\sim$2 km^2) watershed with different wood-debris flow interactions to see what effects these interactions have on the entire distribution of simulated debris flow runout lengths over century timescales.

[7] Throughout this paper we frequently draw upon field observations to guide model construction and help us understand the simulation results, and we use the simulation results to guide our interpretation of the field data. We compare simulated and observed (natural) distributions of debris flow runout lengths in the same basin to calibrate our model and estimate the effects of wood removal on debris flow runout lengths, depositional pattern, and sediment output regime. We also compare our observed distribution to (1) observed distributions from other sites near our field study area to determine whether our results are typical of other, similar areas [*Benda and Cundy*, 1990; *Robison et al.*, 1999] and (2) the distribution predicted by an empirical model to serve as a reference point for our results to a model that is commonly used to assess debris flow impacts and hazards in the Pacific Northwest [*Benda and Cundy*, 1990].

[8] Results show that the effects of wood as outlined above significantly shorten simulated runout lengths. For the calibrated simulation we compare simulated and natural wood constituent fractions and wood quantities to show that the simulated wood masses are realistic. Finally we explore the implications of wood's effect on runout length for sediment yield and distribution within a watershed. While wood cannot affect sediment yield over long timescales of mountain belt exhumation, it can enhance the shorter-term (even millennial scale) sediment capacitance of small watersheds by forming sediment storage reservoirs on the valley floor [e.g., *Swanson and Lienkaemper*, 1978; *Massong and Montgomery*, 2000; *Lancaster et al.*, 2001; *Montgomery et al.*, 2003] (Figure 1). Also, if woody debris flows have shorter runout lengths, then removal of wood may change not only the short term   de of sediment yield but also

the dominant transport process, i.e., fluvial or mass movement, by which sediment leaves a given watershed.

2. Study Area in the Oregon Coast Range

[9] Field and modeling work were both sited in a 2.1-km^2 tributary to Hoffman Creek in the Oregon Coast Range (Figure 2). The basin is small enough to study and model and large enough to exhibit network-scale effects and has no mid-slope or valley-bottom roads to complicate the history of mass movements. It is underlain by massive, gently dipping beds of the Eocene Tyee sandstone formation [*Peck*, 1961]. Topography is steep (valley sideslopes are typically $\sim$40°) and highly dissected with elevations ranging from 10 m to 265 m above sea level. Soils are relatively shallow, highly porous (Table 1), and have low bulk densities (e.g., *Reneau and Dietrich* [1991] measured values of $\sim$1 kg/m^3 at a similar site in the Oregon Coast Range). The climate is maritime with warm, dry summers and mild, wet winters and mean annual precipitation of approximately 1800 mm [*Oregon Climate Service*, 1990]. Diffusive hillslope transport processes and debris flows deliver sediment to the valley network [e.g., *Dietrich and Dunne*, 1978; *Benda*, 1990], with the latter process becoming dominant in the larger valleys of the study area. Field and modeling studies of soil production and transport [*Reneau et al.*, 1989; *Reneau and Dietrich*, 1991; *Roering et al.*, 1999; *Heimsath et al.*, 2001], biomass and root growth and decay [*Harmon et al.*, 1986; *Sidle*, 1992; *Benda and Dunne*, 1997], landslide initiation [*Montgomery and Dietrich*, 1994; *Dietrich et al.*, 1995; *Montgomery et al.*, 2000], and debris flow runout [*Iverson*, 1997; *Iverson and Denlinger*, 2001] provide parameter values appropriate for the study area (Table 1) and guidance in the development and implementation of submodels appropriate for the present study.

[10] The area is forested with primary species Douglas fir (*Pseudotsuga menziesii*) and secondary species western hemlock (*Tsuga heterophylla*), western red cedar (*Thuja plicata*), red alder (*Alnus rubra*), big leaf maple (*Acer macrophyllum*) and vine maple (*Acer circinatum*). Nearly half of the basin was harvested circa 1965, but large quantities of wood were left in low-order channels as large, cut logs. In this part of the Oregon Coast Range, forest surficial biomass is typically less than but of the same order of magnitude as the mass of the soil layer, especially in mature stands [*Grier and Logan*, 1977; *Sidle*, 1992; *Duan*, 1996; *Heimsath et al.*, 2001]. Wood is therefore a significant part of the mass moved by landslides and debris flows.

3. Modeling Methods, Assumptions, and Initialization

[11] Debris flows originate on hillslopes, which provide the initial "debris", i.e., sediment, water, and wood, and travel through the stream network, where they accumulate more debris until they stop. A model simulating many debris flows in a drainage basin over a long time must therefore also include mechanisms for (1) sediment production from the parent material, i.e., conversion of bedrock to soil; (2) delivery of that sediment to potential failure sites and the valley via slope-dependent transport processes; (3) biomass growth and delivery to failure sites and the valley via tree fall; (4) delivery of water to failure sites and the

Table 1. Parameters, Values, and Sources

Parameter	Value	Source
Soil storage porosity	0.624	*Reneau and Dietrich* [1991]
Soil flow effective porosity, n_{eff}	0.05	hypothesized
Alluvial porosity	0.40	*Hough* [1957]
Soil cohesion, C_s	500 Pa	*Schroeder and Alto* [1983]
Soil saturated bulk density	1620 kg/m^3	*Reneau and Dietrich* [1991]
Sediment and soil grain density	2660 kg/m^3	*Reneau and Dietrich* [1991]
Soil and alluvial diffusivity	5.0×10^{-3} m^2/yr	*Reneau et al.* [1989]; *Roering et al.* [1999]
Soil production rate at zero depth, decay scale	2.8×10^{-4} m/yr, 0.3 m	*Heimsath et al.* [2001]
Soil saturated hydraulic conductivity, K_s	1.0×10^{-3} m/s	calibrated
Alluvial saturated hydraulic conductivity	1.0×10^{-4} m/s	*Montgomery et al.* [1997]
Mean rainfall intensity and duration	1.7 mm/hr, 20 hrs	*Benda and Dunne* [1997]
Mean interstorm duration	5 days	*Duan* [1996]
Downstream hydraulic width exponent, coefficient	0.5, 7.0 m/(m^3/s)$^{1/2}$	OCR mean annual flow versus width data
At-a-station hydraulic width exponent	0.25	*Leopold and Maddock* [1953]
Downstream hydraulic roughness exponent, coefficient	−0.01, 0.03	*Leopold and Maddock* [1953]
At-a-station hydraulic roughness exponent	−0.21	*Leopold and Maddock* [1953]
Channel drainage area threshold	1.0×10^4 m^2	field verified
Exponents for fluvial transport capacity, m_f, n_f, and p_f	0.6, 0.7, 3.0	*Tucker et al.* [2001b]
Fluvial transport coefficient, K_f	1.0×10^{-3} m^{5}s^5/kg^3	hypothesized
Critical shear stress for fluvial transport, τ_c	0	hypothesized
Internal and bed slip friction angles, ϕ_i, ϕ_b	42°, 28°	*Iverson* [1997]
Maximum time step for debris flow motion	0.1 s	arbitrary
Maximum root strength	14 kPa	*Burroughs and Thomas* [1977]
Ratio of lateral and vertical root strength, m	2.33	*Burroughs* [1984]; *Hammond et al.* [1992]
Root and biomass growth constants	0.95, 19.05, −0.05	*Sidle* [1992]
Root growth time constant	0.25 yr^{-1}	*Sidle* [1992]
Root decay time constant and exponent	0.5 yr^{-1}, 0.73	*Burroughs and Thomas* [1977]; *Benda and Dunne* [1997]
Root strength depth constant	2.0 m^{-1}	*Benda and Dunne* [1997]
Tree height index	40 m	*Means and Sabin* [1989]
Maximum biomass weight	3.00 kPa	*Sidle* [1992]; *Duan* [1996]
Biomass time constant	0.12 yr^{-1}	*Sidle* [1991]
Tree diameter constants, b_0, b_1, and b_2	74.0 m, −0.0105 m^{-1}, 0.911	*Garman et al.* [1995]
Wood decay constant	0.031 yr^{-1}	*Harmon et al.* [1986]
Wood density	450 kg/m^3	
Blowdown parameter	1.0×10^{14} kg/m^3	calibrated
Mean time between fires	200 yr.	*Long et al.* [1998]
Concavity (β) and steepness (K) indexes, $8.5 \times 10^4 \leq A < 10^6$ m^2	0.41, 13.5	field derived and calibrated
Concavity (β) and steepness (K) indexes, $A \geq 10^6$ m^2	1.41, 1.6×10^7	field derived and calibrated
Factor multiplying hydrostatic pore pressure	1.8	calibrated

stream network; and (5) landslide initiation. Since forest dynamics play a vital role in the timing and location of, and volume of wood in, mass movements, that interaction should be included as well.

[12] Our model is an extension of the Channel-Hillslope Integrated Landscape Development (CHILD) model [*Lancaster*, 1998; *Tucker et al.*, 2001a, 2001b]. As such, the present model operates on a Delaunay [e.g., *Du*, 1996] triangulated irregular network (TIN), which has an associated Voronoi diagram, i.e., the inverse of the triangulation that defines the (Voronoi) areas closest to each node (Figure 3), and shares the CHILD model's drainage area calculation algorithm and stochastic precipitation and runoff generation models. A similar model was used by *Lancaster et al.* [2001], but the version presented and fully explained here is significantly different.

3.1. Landscape and Storm Characteristics

[13] The model uses gridded digital elevation model (DEM) data with 10-m discretization to interpolate the elevations of the nodes in the TIN. The DEM resolves some features missed by USGS DEMs with 30-m discretization, but other features, such as small hollows, e.g., those less than 20–30 m across and 5–10 m deep are still unresolved. Node locations are random   minate grid bias and form a

TIN with the same average discretization as the original DEM. Additional points are added at large drainage areas to eliminate "jaggy" channels typical of interpolated TINs. Finally, channel-adjacent nodes that would fall within channels are removed [*Lancaster*, 1998]. Nodes in the landscape are classified according to three types, hillslope, channel, and valley nodes (Figure 3). Elevations of hillslope nodes are static because any model-driven changes would only decrease the accuracy of topographically driven transport processes [*Dietrich et al.*, 1995]. Channel and valley node elevations evolve over time in response to aggradation and evacuation of sediment and wood because fluvial processes are sensitive to these fluctuations, but bedrock elevations are held static for channel and valley nodes. Nodes' designations are dynamic, changing as the position of the channel changes in response to changes in valley topography due to deposition or erosion. Thus hillslope and valley nodes may become channel nodes, and abandoned channel nodes become valley nodes.

[14] The model is fed a stochastic time series of storms based on the work of *Eagleson* [1978], as in the works of *Benda and Dunne* [1997], *Duan et al.* [1998], *Tucker and Bras* [2000], and *Tucker et al.* [2001b]. The parameters of the stochastic model were derived from storm data for the Oregon Coast Range [*Benda and Dunne*, 1997] or else-
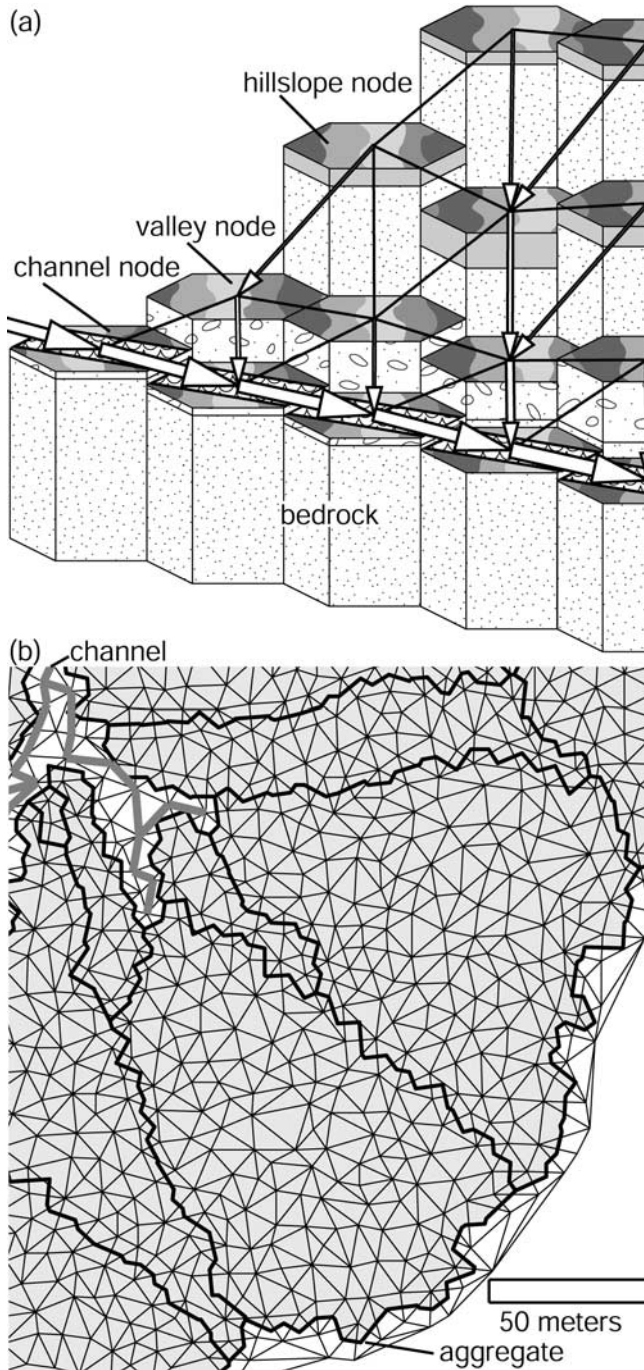
where in western Oregon [*Duan et al.*, 1998] (Table 1).The storms drive landslide initiation, fluvial transport, and tree fall, discussed below. The model records debris flow runout paths and deposited depths of wood and sediment at each point in the channel and valley network. An important feature of the model is that the history of previous events bears directly on later ones: areas that fail have their soil volumes removed, runout paths are scoured of wood and sediment or have wood and sediment deposited, and subsequent debris flows encounter previous deposits, which may change channel and valley gradients and act as barriers.

[15] In the model, the sediment eventually moved by debris flows originates as hillslope soil, defined here as material lacking the structure of the underlying bedrock. Soil depths on the hillslopes are governed by soil production and transport, where the soil production rate at a point decreases exponentially with the soil depth and transport is modeled with linear diffusion [*Heimsath et al.*, 1997, 2001]. Diffusion and soil production parameter values have been measured in the Oregon Coast Range [*Reneau et al.*, 1989; *Roering et al.*, 1999; *Heimsath et al.*, 2001] (Table 1). Though hillslope elevations do not change, soil depths evolve over time. Soil production is only active on the hillslopes, but diffusion acts on all landscape nodes and thus may transport material among hillslope, valley and channel nodes. Diffusion of material from a node is contingent on supply: bedrock does not diffuse.

[16] Channels are defined as nodes with a drainage area exceeding a threshold determined from analysis of slope-area plots [e.g., *Tarboton et al.*, 1991; *Ijjasz-Vasquez and Bras*, 1995] and trial and error. Channel source area values from field measurements [*Montgomery and Dietrich*, 1988, 1992] produce a channel network with "feathered" extremities on our relatively coarse DEM [*Montgomery and Foufoula-Georgiou*, 1993]. We found a contributing area threshold of 10^4 m^2 was large enough to avoid such feathering and small enough to capture some of the debris flow-scour-dominated part of the channel network, recognizable by relatively little decrease in gradient with increasing contributing area [*Stock and Dietrich*, 2003]. Through field reconnaissance we found that this threshold may exclude some small channels but effectively marks the transition from bowl-shaped hollows to V-shaped valleys. Drainage area is determined by routing each node's area downstream in the direction of steepest descent.

[17] In the channel network, transport of total sediment load is limited by transport capacity, which is represented by a power law of excess shear stress, where shear stress is represented by a power law of unit discharge and local slope derived from continuity and the Manning equation:

$$Q_s \leq K_f b_h \left[\rho_w g \left(\frac{Qn}{b_h} \right)^{m_f} S^{n_f} - \tau_c \right]^{p_f} \qquad (1)$$

where Q_s is potential sediment discharge, i.e., contingent on supply; K_f, m_f, n_f, and p_f are constants; b_h is hydraulic width; Q is water discharge; n is Manning's hydraulic roughness; S is hydraulic slope; ρ_w is water density; g is gravitational acceleration; and τ_c is critical shear stress [*Tucker et al.*, 2001b] (Table 1). Discharge is generated by saturation overland flow, as in the works of *Tucker and Bras* [2000] and *Tucker et al.* [2001b], such that alluvial depth in the channel affects discharge, and hydraulic width and rough-

Figure 3. (a) Schematic diagram of nodes, mesh, and flow routing. Nodes are connected by edges of Delaunay triangular mesh and have associated Voronoi areas, i.e., area closer than to any other node. Each Voronoi area is a polygon composed of Voronoi edges, which are perpendicular bisectors of the edges of the Delaunay triangles. Flow follows steepest edges ("flow edges") to neighboring nodes (arrows). Hillslope nodes have vegetation and soil overlying bedrock; channel and valley nodes have vegetation and alluvium overlying bedrock; and channel nodes contain a channel segment. (b) Part of irregular mesh showing aggregates of hillslope nodes (shaded) and channels (thick shaded line). Nodes neither within an aggregate nor connected to a channel segment are valley nodes.

ness are calculated from empirical power laws of discharge, both downstream and at a station [*Tucker et al.*, 2001b] (Table 1). Equation (1) represents total load, i.e., both suspended and bed load, for values of p_f in the range of 2.5–4.5 [*Engelund and Hansen*, 1972; *Vanoni*, 1975; *Garde and Ranga Raju*, 1985; *Govers*, 1992]. This transport law has not been calibrated for streams in the Oregon Coast Range. Rather, it is simple and generic. The most salient feature of equation (1) for the present study is the dependence on local hydraulic slope, which changes during the simulation as a result of sediment and wood aggradation and scour. Our observations indicate that the small streams in the study area are not competent to remove wood from debris flow deposits, and these observations are consistent with findings of *Lienkaemper and Swanson* [1987]. Therefore we assume that wood cannot be transported by fluvial processes, so until they decay wood deposits act as barriers to sediment transport by decreasing upstream slope.

3.2. Landslide Initiation

[18] Landslide initiation occurs when rainfall exceeds a duration-dependent intensity. Our formulation of this critical precipitation for possible failure is based on the Mohr-Coulomb criterion for failure of an infinite slope as developed by *Montgomery and Dietrich* [1994] and *Dietrich et al.* [1995] and lies somewhere between the two in complexity, similar to *Montgomery et al.* [2000]. We assume uniform saturated hydraulic conductivity within the soil layer and zero conductivity beneath that layer. The critical precipitation, P_{cr}, is given by

$$P_{cr} = \frac{K_s H b_V \cos\theta \sin\theta \rho_b}{A_{eff} \rho_w}\left[1 - \frac{1}{\tan\phi_i}\left(\tan\theta - \frac{C_r + C_s}{H\rho_b g \cos^2\theta}\right)\right]$$
(2)

where K_s is saturated soil hydraulic conductivity; H is vertical soil thickness plus, in cases where wood is incorporated by debris flows, equivalent depth of wood in standing and fallen trees; b_V is the length of the Voronoi edge perpendicular to the "flow edge" (Figure 3); θ is slope angle; ρ_b is bulk density of the failing soil and wood, assuming saturated bulk density for the soil; A_{eff} is effective area contributing to flow and is dependent on storm duration; ϕ_i is internal friction angle; C_r is root cohesion or strength; and C_s is soil cohesion (Table 1). Root strength is added as an apparent cohesion to the infinite-slope stability model as in the work of, e.g., *Selby* [1993], *Dietrich et al.* [1995], *Wu and Sidle* [1995], and *Benda and Dunne* [1997] and accounts for both vertical (basal) cohesion and lateral strength as in the work of *Benda and Dunne* [1997] but does not deal explicitly with the geometry of the failure scarp as in the work of *Montgomery et al.* [2000] and *Schmidt et al.* [2001]. We derived a simple expression for the effective area contributing to flow, A_{eff}, by solving the Darcy equation for an effective upslope length contributing to subsurface flow during a storm of known duration, t_d, and squaring that length to get A_{eff}:

$$A_{eff} = min\left[\left(\frac{t_d K_s \sin\theta}{n_{eff}}\right)^2, A\right]$$
(3)

where A is topographically defined contributing area; and n_{eff} is the effective porosity for subsurface flow, which field experiments have shown   ch smaller than the actual

porosity (Table 1), i.e., the actual travel time is much smaller than that calculated from the actual porosity, most likely because the experiments are actually measuring the arrival of a peak in discharge rather than of the water itself [*Iverson et al.*, 1997; *Montgomery et al.*, 1997]. Using A_{eff} accounts for greater saturation during longer storms but does not account for transient pore pressure increases from short, intense rainfall periods during longer storms. Such transient increases may be responsible for many natural failures [*Montgomery et al.*, 1997; *Torres et al.*, 1998; *Iverson*, 2000].

[19] Critical precipitation is directly proportional to saturated hydraulic conductivity, K_s, which may vary over orders of magnitude between sites and even within relatively small regions in the field [*Duan*, 1996]. Because the amount of sediment delivered to the channel network by debris flows is ultimately limited by the soil production rate, K_s will mainly affect soil depths and the ratio of sediment to wood in debris flows by allowing, or not, realistic amounts of soil to accumulate before failing. We calibrated, albeit roughly, saturated hydraulic conductivity by running several simulations on a small part of the study area while varying the order of magnitude of K_s within the range of reported values and selecting the value that produced reasonable average soil depths on the hillslopes ($\sim$0.5 m) [*Montgomery et al.*, 1997; *Heimsath et al.*, 2001] (Table 1).

3.3. Debris Flows

[20] When landslides occur, the associated sediment, wood, and water from failing hillslope nodes move as debris flows. To describe debris flow runout, we use a physically-based debris flow model that is simplified to run within the landscape-scale model. To this basic runout model are added rules and criteria for entrainment of materials in the debris flow's path, stability of deposits, and response to changes in valley geometry.

3.3.1. Momentum Conservation Equation for Runout

[21] *Iverson* [1997] and *Iverson and Denlinger* [2001] developed models describing debris flow runout as an evolving waveform with mixture theory and depth-averaged conservation of mass and momentum in two and three dimensions, respectively. Those models use fixed sets of nodes that cover the entire runout zone, from initiation site to deposition. Such a scheme is computationally infeasible on the network scale and would, in any case, require better topographic data than is available. We use a simplified form of the *Iverson and Denlinger* [2001] equation for conservation of momentum in the direction of flow. For feasibility, we neglect several terms in the momentum balance: convective accelerations; longitudinal normal stresses that characterize interaction between debris flow head and tail; transverse shear stresses that characterize debris flow interaction with lateral boundaries; multidimensional momentum transfers arising from the fact that velocity is a vector quantity; and, among the basal shear stresses, the term arising from fluid viscosity. Except for the convective accelerations, nondimensionalization indicates that the neglected terms are relatively small, although these terms can actually be quite important [*Iverson and Denlinger*, 2001]. We also neglect additional constraints imposed by multidimensional mass conservation. Instead, we treat debris flow motion as a one-dimensional point process, where that point moves with the front of the flow, and velocity and depth are functions only

of time. Such a simplified treatment necessitates neglecting the convective accelerations. By eliminating the terms noted above and thereby reducing the equations of *Iverson and Denlinger* [2001], conservation of momentum in the flow direction is then given by:

$$\frac{d}{dt}(\rho h v) = -\text{sgn } v (\rho h g \cos \theta - p_b) \left(1 + \frac{v^2}{g \cos \theta} \frac{d\theta}{ds}\right) \tan \phi_b$$
$$+ \rho h g \sin \theta \quad (4)$$

where h is slope-normal debris flow depth; v is slope-parallel debris flow velocity; t is time; p_b is pore pressure at the bed; ρ is debris flow mixture density, which is updated at every time step from the relative proportions and densities of the constituents, sediment, water, and wood (Table 1); s is the slope-parallel direction; ϕ_b is bed friction angle (Table 1); and the factor, $-\text{sgn } v$, indicates the direction opposite that of the debris flow velocity. The left-hand side represents changes in momentum per unit area and can be expanded according to the chain rule to explicitly represent changes in flow density, depth, and velocity. Changes in density and depth are prescribed by entrainment of sediment, wood, and water and changes in channel and valley geometry, as explained below, so equation (4) is solved for the change in velocity. The first group of terms on the right-hand side is the basal shear stresses resisting motion and therefore acts in the direction opposite the flow direction. The terms within the first set of parentheses represent the effective normal stress on the flow in the absence of acceleration, i.e., the component of the gravitational stress normal to the slope minus pore pressure at the bed. The terms in the second set of parentheses represent the modification of the normal stress by centripetal acceleration due to changes in slope angle. The effective normal stress is multiplied by the basal Coulomb friction angle to obtain the component of the normal stress resisting motion. The resisting shear stress is constrained to be negative, i.e., large pore pressure or negative centripetal acceleration cannot lead to the resisting stress becoming an impelling stress. In using flume-derived values for bed friction, we are assuming that the smooth flume is similar to the smooth Tyee sandstone in the study area and neglecting other, unknown contributions to friction. The last term on the right-hand side represents the impelling shear stress, the slope-parallel component of the gravitational stress.

[22] The experimental measurements of *Iverson* [1997], *Iverson et al.* [1997], *Reid et al.* [1997], and *Major and Iverson* [1999] indicate that although pore pressure at the front and edges of the flow is typically near hydrostatic, pore pressure in the main body of the flow typically increases to nearly compensate for the total normal force, advects with the flow, and then diffuses over times that are large relative to the time between initiation and deposition. *Denlinger and Iverson* [2001] employ this result by assuming that the pore pressure soon after initiation of debris flow motion rises to 0.9 of the normal stress. For the saturated sediment used in the experiments of *Iverson et al.* [1997] and *Reid et al.* [1997] this increase in pore pressure corresponds to multiplying the hydrostatic pressure by a factor of 1.8. We use this result as a basis for calibrating our own model's debris flow runout length distribution to the observed distribution in the study area, as explained later. Given the simplificatio   our model, we must also

assume a uniform pore pressure in the mixture. In our calculation of hydrostatic pore pressure we assume the sediment constituent porosity is no less than the alluvial porosity (Table 1).

3.3.2. Entrainment- and Valley Geometry-Induced Depth Changes

[23] Although we neglect spatially varying terms in the mass conservation equation, continuity does require temporal changes in depth due to addition of material through scour and changes in flow width. *Iverson* [1997] and *Iverson and Denlinger* [2001] assumed constant debris volume with time but allowed depth and velocity to coevolve. In the field, the effects on runout of increases in debris flow volume during runout are substantial. *May* [1998] found that on the order of half of debris flow deposit volumes that she measured in the Oregon Coast Range were from entrainment during runout, and other studies indicate that the fraction may be even larger [*Benda and Cundy*, 1990; *Benda*, 1990]. Scour of sediment from previous deposits is important but poorly constrained.

[24] *Kuang et al.* [1998] found that "ripping up the bottom" by hyperconcentrated flows could be represented by considering the balance of forces at the scour depth as imparted by the overburden of the hyperconcentrated flow and the bed material itself. We employ a similar analysis here to find the minimum depth of bed material that will "fail" given the overburden of a debris flow in motion. Scour of the substrate occurs where the sum of impelling and resisting stresses results in net impelling stress, similar to slope failure, i.e.,

$$\tau_{imp} + \tau_{res} \geq 0. \quad (5)$$

The impelling stress on the substrate is given by the sum of the slope-parallel gravitational stresses on the debris flow and substrate:

$$\tau_{imp} = (\rho_b h_e + \rho h) g \sin \theta \quad (6)$$

where ρ_b is the bulk density of the substrate and h_e is the slope-normal depth of substrate erosion. The resisting stress is given by the sum of the frictional component of normal stresses on the debris flow and substrate and apparent cohesion:

$$\tau_{res} = -\left\{\left[\rho_b h_e + \rho h \left(1 + \frac{v^2}{g \cos \theta} \frac{d\theta}{ds}\right)\right] g \cos \theta - \rho_w g \cos \theta (h_e - h_w)\right\}$$
$$\cdot \tan \phi_i - (C_r + C_s) \quad (7)$$

where h_w is the slope-normal depth to the water table from the substrate surface. The first group of terms in the curly brackets is the normal stress due to the weight of the substrate and the debris flow, where the latter is modified by centripetal acceleration because it is in motion. The second group of terms in the curly brackets is the hydrostatic pore pressure at the depth of substrate failure, h_e. As in slope failure, the effective cohesion is given by the sum of "soil" cohesion and apparent root cohesion. In practice, we neglect soil cohesion because the substrate may be either soil or valley deposit, and cohesion for the latter is unknown.

[25] Note that we assume substrate pore pressure is unaffected by the pore fluid of the debris flow. This

assumption is based on comparison of pore pressure diffusion and debris flow motion timescales. The pore pressure diffusion timescale as defined by *Iverson* [2000] for scour depths of 0.1–1.0 m and typical diffusivity for shallow rapid failures, 10^{-3} m²/s, is 3–300 s. We define the timescale of debris flow motion as the ratio of length to velocity. For typical length and velocity in our simulations of 10 m and 10 m/s, respectively, this timescale is 1 s, which is less than the pore pressure diffusivity timescale. On the basis of this comparison, our assumption that debris flow fluid does not affect pore pressure at the scour depth is valid, although this assumption might become invalid for shallower scour depths and longer and slower debris flows.

[26] Substituting equations (6) and (7) into equation (5) and solving for the minimum scour depth, h_e, we get

$$h_e \geq \frac{\rho h \left(1 + \dfrac{v^2}{g\cos\theta}\dfrac{d\theta}{ds} - \dfrac{\tan\theta}{\tan\phi_i}\right) + \rho_w h_w + \dfrac{(C_r + C_s)}{g\cos\theta\tan\phi_i}}{\rho_w - \rho_b\left(1 - \dfrac{\tan\theta}{\tan\phi_i}\right)} \quad (8)$$

For a debris flow 1 m deep with zero velocity, debris flow and substrate density equal to the saturated soil bulk density of 1620 kg/m³, $\phi_i = 42°$ (Table 1), zero depth to the water table, h_w, and zero cohesion, $h_e \to \infty$ as $\theta \to 19°$ from above, is positive and decreasing with increasing θ for $19° < \theta < \phi_i$, and negative for $\theta > \phi_i$, i.e., any finite depth is unstable above the angle of repose. Larger values as slope angle decreases indicate that greater depths of saturated soil are required for failure at lower slope angles and that as slope angle decreases to approach a threshold value, 19° in this special case, failure and therefore scour become impossible. This threshold angle for erosion is significantly larger than the value of approximately 10° observed in the field by, e.g., *Benda and Cundy* [1990] and *May* [2001], a discrepancy that is likely due to our neglecting drag forces associated with grain impacts and sliding friction. We employ equation (8) despite its shortcomings rather than introduce unconstrained parameters and because it allows us to find entrainment at a node upon debris flow arrival. The benefit of this latter characteristic will become apparent when we explain implementation of the debris flow model below. Also, although we have found some channels with slopes less than 19° scoured to bedrock by debris flows in the Hoffman Creek study area, most channels scoured by debris flows are steeper, and we found many debris flow deposits in channels steeper than 19°. The above criterion, equation (8), is used to determine whether the substrate, which is generally composed of sediment, water, and wood, at a point is thick enough to fail and be entrained by the debris flow. Water flowing on the surface is automatically entrained by the debris flow and does not affect the calculation in equation (8), i.e., the depth to the water table, h_w, cannot be negative.

[27] Debris flow width is determined by the flow depth and local channel, node, and valley geometry (Figure 4), and changes in flow width affect depth, i.e.,

$$h_{new} = h_{old}\left(b_{old/b_{new}}\right). \quad (9)$$

A debris flow may widen to cover, at most, only one node before reaching a channel or valley node for the first time and, thereafter, three nod   ., the node to which the
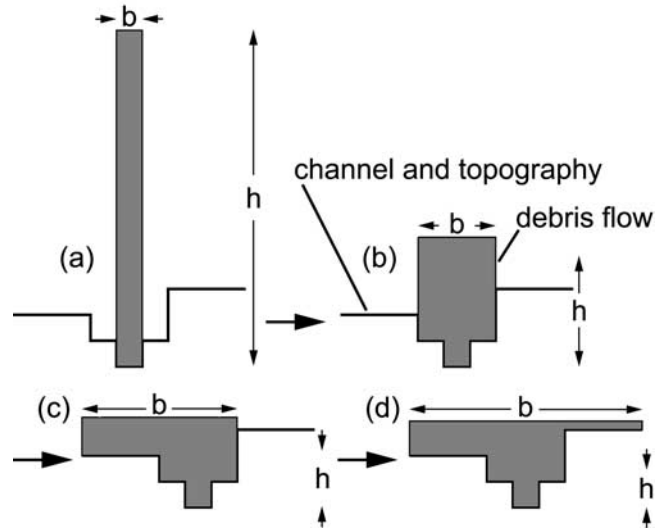

Figure 4. Schematic diagram illustrating the calculation of debris flow width, b, and depth, h, given the channel and valley geometry. If the flow is deep enough, it can overflow the channel (a) and spread to occupy: the average width of the channel node (b); that width plus the average width of the bank node with the lower elevation or "bank height" (c); and, finally, that width plus the average width of the bank node with the higher elevation (d). The two bank nodes, one each on the right and the left, are neighbors connected by the edges that are most nearly perpendicular to the flow edge (Figure 3). The flow depth used in equation (4) is the average depth, i.e., the material volume divided by the length and width. Average channel node width is the node's Voronoi area divided by the length of the flow edge. Average width of a bank node is that node's Voronoi area divided by the length of the channel node's flow edge.

debris flow is routed plus one "bank node" on either side (Figure 4). Separate erosion calculations using the slope at the center node are done for the banks if the debris flow covers one or both banks.

3.3.3. Deposition

[28] In one sense, debris flow deposition is simple: it occurs when velocity goes to zero. The fact of deposition, however, does not tell us the configuration of the final deposit, i.e., its depth and length. Without some criterion for calculating that configuration, the model could produce debris flow deposits of arbitrary and unrealistic thickness. For that criterion, we once again employ the infinite slope model for Mohr-Coulomb failure. This approach is suggested by the observations of *Miyazawa* [1998]. For a deposit of vertical thickness, H, and a failure plane at vertical depth, H_e, and zero cohesion (likely a good assumption for a fluidized mixture), the criterion for failure becomes,

$$\frac{\rho H_e \tan\phi_i + \rho_w(H_w - H_e)\tan\phi_i}{\rho H_e\left(\tan\theta + \dfrac{H - H_e}{\Delta x}\right)} = 1 \quad (10)$$

where H_w is the vertical depth to the "water table"; θ is the slope angle of the channel or valley floor beneath the deposit; Δx is the horizontal distance to the downstream

node; and the term in parentheses in the denominator represents the slope at the failure depth. For purposes of determining deposit failure, we assume that any wood in the debris flow floats on top of the other constituents so that when the debris flow contains wood, H_w will be at least the depth to the bottom of the wood constituent. We assume that the minimum porosity of the sediment constituent is the alluvial porosity (Table 1) so that H_w will be larger than the depth to the bottom of the wood constituent if the water constituent is not great enough to fill that minimum pore space of the solid constituent. Equation (10) can be rearranged to form an equation that is quadratic with respect to H_e:

$$\left(\frac{\rho}{\Delta x}\right)H_e^2 + \left[(\rho - \rho_w)\tan\phi_i - \rho\left(\tan\theta + \frac{H}{\Delta x}\right)\right]H_e + \rho_w H_w \tan\phi_i = 0$$

(11)

which can be solved for H_e if real solutions exist. If equation (11) has two positive solutions where $H_e \leq H$, then we choose the larger solution, but the failure depth must be larger than the depth to the bottom of the wood constituent for failure to occur, i.e., the failure plane cannot be within the "column" of wood at the top of the debris flow. If the new deposit covers one or both banks and refailure occurs, the material covering the banks also fails to the depth of the banks or the failure depth, whichever is smaller.

3.3.4. Incorporation of Wood in the Runout Model

[29] Unlike any other debris flow runout model that we are aware of, ours incorporates all three major constituents observed in the study area: sediment, water, and wood. The above model is sufficient to model debris flows unaffected by wood. Here, we explain how the model deals with two hypothesized effects of wood.

3.3.4.1. Velocity Reduction due to Wood Entrainment and Acceleration

[30] As with sediment, debris flows must accelerate wood entrained during runout. The observation that debris flows bulldoze surface wood suggests that we may simply model this kind of wood entrainment by enforcing a rule that debris flows entrain all surface wood, i.e., standing and fallen, in their paths. This rule and equation (4) can force a debris flow to stop if enough wood lies in its path that the debris flow lacks the momentum to force the wood into motion. This rule cannot account for wood's resistance to breaking when firmly anchored, e.g., if spanning and wedged between bedrock valley walls. Entrainment of wood from deposits is, like sediment, subject to equation (8). Wood contributes to the calculation of the bulk density and is assumed to have zero porosity.

3.3.4.2. Velocity Reduction at Bends

[31] Debris flows composed of sediment and water typically travel through bends with smooth curvature [e.g., *Iverson et al.*, 1994] with little loss of velocity (R.M. Iverson, USGS Cascades Volcano Observatory, personal communication, 2002). For woody debris flows, we observe in the study area and other locations in the Oregon Coast Range that large changes in flow direction are typically associated with deposition, and this observation is common in the Pacific Northwest, especially the Oregon Coast Range [e.g., *Benda and Cundy*, 1990; *Robison et al.*, 1999]. However, our observations indicate that a single threshold angle for deposition, as   work of *Benda and Cundy*

[1990], is inappropriate but, rather, the likelihood of a debris flow continuing through a large-angle bend is greater where the runout length upstream of that turn is greater, i.e., when the debris flow has a longer period of acceleration before encountering the large-angle bend (see results below). These observations indicate that bends decrease debris flow velocity. To account for these observations in the model, we treat woody debris flows traveling through bends as collisions between debris flow masses and outgoing valley walls. These collisions are inelastic in the direction normal to the outgoing direction such that debris flows' outgoing velocities are constrained to be parallel to outgoing valley walls. Given the above constraints and that valley wall masses are much greater than the debris flow masses, conservation of momentum dictates that the outgoing velocity of the coupled valley wall-debris flow pair is zero in the direction normal to the outgoing valley wall and equal to the component of the incoming velocity parallel to the outgoing direction in the outgoing wall-parallel direction, i.e., the incoming (v_{in}) and outgoing (v_{out}) velocity magnitudes are related as

$$v_{out} = v_{in}\cos\alpha$$

(12)

where α is the angle between the new and old downstream directions in the horizontal plane. At a given node, α is calculated over a spacing of several nodes (>30 m) both upstream and downstream so that this rule is independent, to a point, of path discretization scale. Because debris flow length is held constant, such changes in velocity do not lead to changes in depth and therefore length.

[32] Simulations with and without each of the above proposed rules concerning wood, as well as with and without both of them, will clearly show their effects, singly and in combination, on simulated debris flow runout lengths.

3.3.5. Implementation of Debris Flow Model

[33] Debris flows automatically travel from node to node in the landscape mesh in the direction of steepest descent. Landslide initiation and debris flow runout are processed in a separate step during storms, after fluvial transport has been calculated. Landslide initiation sites are found by applying the initiation criterion, equation (2), to each hillslope node. The resulting debris flows are processed in order from initiations at larger to smaller drainage areas so that debris flows originating at larger drainage areas, i.e., those further downslope, run out before those coming from upslope. Each debris flow "sees" the channel and valley topography as changed by the previously processed debris flows.

[34] Initial debris flow depth is the sum of the constituent depths at the initiating node, and density is the weighted average of the constituent densities, as in the work of *Iverson and Denlinger* [2001]. Initial debris flow length is equal to the slope-parallel length of the flow edge at the initiating node, and the initial width is the node's area divided by the debris flow length. Upon initiation, an initial acceleration is calculated assuming no changes in depth or density, and that acceleration yields the initial debris flow velocity for debris flow processing, which takes over at the next node downstream.

[35] When a debris flow reaches a new node, velocity reduction due to the bend angle, if applicable, is calculated

first according to equation (12). Changes in depth, density, and width that will occur while traversing that node are calculated (length is held constant) before calculation of change in velocity due to momentum conservation and thus change in position because the rates of depth and density change are needed to solve equation (4) for velocity change. The amount of new material to be entrained is calculated, first, from the rules that all surface water and wood, if wood is to be incorporated, are automatically entrained and, second, from erosion, if any, of the substrate as calculated from equation (8). Change in width is calculated based on (1) changing geometry between the current node and the next node downstream (e.g., changing node size on hillslopes or changing channel, node, and valley geometry in the valley; Figure 4) and (2) the present and projected, i.e., present plus entrained, material volumes. Changes in total and constituent depths, then, are the differences between present and projected average depths based on present and projected material volumes and flow widths. Finally, the time step for the numerical solution of equation (4) is set to 1/10 of the time for the debris flow to traverse the node's flow edge at its initial velocity at that node (i.e., after using equation (12) if applicable), although a maximum time step (Table 1) is set to insure that debris flows accelerating from low velocities will not "overshoot" the end of the flow edge.

[36] Next, the depth, density, velocity, and position are calculated at each time step until the debris flow reaches the end of the current flow edge. First, the rates of change of total and constituent depth and total width are calculated from the current velocity, the remaining depth and width changes, and the remaining distance to the next node. Second, total and constituent depths and total width, as well as amounts of change remaining, are updated according to the current rates of change. Third, the mixture density, ρ, is updated with the new constituent and total depths. Fourth, the velocity is updated by using the chain rule to expand the left hand side of equation (4) and solving it for the velocity change. Finally, the remaining distance to the next node is decremented. These time stepped calculations continue until that remaining distance or the velocity goes to zero. If the remaining distance goes to zero, then the debris flow has arrived at a new node, and the above procedures are repeated.

[37] If the velocity goes to zero, then the debris flow has stopped, and the new deposit is tested for partial refailure with equation (11). First, the remaining total and constituent depth and total width changes are added to the debris flow. Second, total and constituent depths and total width are recalculated with any added material and assuming that the length of the new deposit has changed to fit the flow edge where the debris flow has stopped. If the deposit refails, then the continuing debris flow will have this new length, i.e., the slope-parallel length of the current flow edge. Deposit refailure is the only time debris flow length changes during runout.

3.4. Tree Growth, Mortality, and Decay

[38] Trees and wood affect many parts of the model: Wood in channels affects fluvial sediment transport; tree roots affect landslide susceptibility and scour; and the mass of trees and wood on hillslopes and in valleys affects debris flow momentum. We include these effects by modeling: (1) growth and decay of tree   , (2) growth and decay of

wood biomass, (3) wood movement among nodes by tree-fall, and (4) forest death by fires.

[39] The evolution of several variables describing the forest is governed by a set of empirical equations with parameters that vary according to species. We have chosen parameter values representative of Douglas fir (*Pseudotsuga menziesii*), the dominant species in the field area.

[40] Root strength, C_r, evolves according to exponential decay of root strength after stand death and sigmoid-increasing strength, as in the work of *Sidle* [1992] and *Duan* [1996], and partitioning of root strength between vertical and lateral components, with the vertical component decreasing exponentially with soil depth. Wood volume also grows as the stand ages according to the sigmoid function used by *Sidle* [1992] and *Duan* [1996]. Maximum tree height is determined by the *Richards* [1959] equation on a five-parameter base as used by *Duan* [1996]. Maximum tree diameter at breast height (DBH, height = 1.37 m) is determined by solving the empirical function of *Garman et al.* [1995] for height as a function of DBH. We have chosen parameter values that are representative of Douglas fir.

[41] We follow the approach of *Benda and Dunne* [1997] to calculating the evolution of apparent root cohesion. In the model, root strength, C_r, decays exponentially and increases sigmoidally after stand death, as in the work of *Sidle* [1992] and *Duan* [1996], and is partitioned between vertical and lateral components, with the vertical component decreasing exponentially with soil depth, as in the work of *Benda and Dunne* [1997]. Some parameter values used in root strength calculation were derived specifically for the Oregon Coast Range, while others are generic (Table 1). Lateral and vertical components of root strength are summed to get the total root cohesion, C_r, which is added to soil cohesion in equation (2). We have deviated from the approach of *Benda and Dunne* [1997] in some ways. In our model, root strength can decay from an arbitrary value rather than being constrained to decay from the maximum value. Also, we use a differential form so that root strength at the next time step evolves from the present value. Upon stand death, the constants representing "initial" lateral and vertical root strength, C_{V_0} and C_{L_0}, respectively, are reset from the total root strength at the time of death, C_{r_0}, according to a partitioning coefficient, m, which duplicates the relative partitioning of *Benda and Dunne* [1997]:

$$C_{V_0} = \frac{C_{r_0}}{1 + m}, \ \ C_{L_0} = mC_{V_0}. \tag{13}$$

This root strength model neglects scale effects. In reality, larger failure perimeters should have larger lateral root strength [*Montgomery et al.*, 2000], but, in practice, the model does not calculate failure perimeter.

[42] The sigmoid function of *Sidle* [1992] simulates increasing wood volume as the forest ages. Again, our model employs a differential form during evolution so that biomass at the next time step evolves from the present value. Parameter values for this relationship are generic (Table 1). Maximum tree height evolves with time according to a differential form of *Richards*'s [1959] equation on a five-parameter base, as in *Duan* [1996]. The tree height index used in the model was derived for Douglas fir in the Oregon Coast Range [*Means and Sabin*, 1989] (Table 1).

[43] Tree diameter at breast height (D_{bh}, height = 1.37 m) is calculated by inverting an empirical relationship for height as a function of D_{bh} to solve for D_{bh} as a function of maximum tree height, H_w [*Garman et al.*, 1995]:

$$D_{bh} = \frac{1}{b_1} \ln \left[1 - \left(\frac{H_w - H_b}{b_0} \right)^{\frac{1}{b_2}} \right], \quad H_b < H_w \leq b_0$$
$$= 0, \qquad\qquad\qquad H_w \leq H_b \qquad (14)$$

where b_0, b_1, and b_2 are empirical coefficients determined for Douglas fir in the Oregon Coast Range, and H_b is breast height, 1.37 m [*Garman et al.*, 1995]. Tree height may not exceed b_0 so that the argument of the logarithm in equation (14) cannot be negative.

[44] Trees fall via a stochastic blowdown model. The number of trees falling at a given landscape node during each storm is exponentially distributed, and the mean, or expected, number of blowdowns, μ_N, is given by the ratio of the drag force from wind to the resisting strength of roots:

$$\mu_N = \frac{P^2}{C_r} \left(\frac{\rho_a C_d V_R^2}{2B_T} \right) \qquad (15)$$

where P is the storm precipitation rate; C_r is the root strength; ρ_a is the density of air; C_d is the drag coefficient; V_R is the ratio of storm wind velocity to precipitation rate, i.e., we assume a constant, linear relationship between the two; B_T is the ratio of tree crown width (i.e., the cross-sectional area presented to the wind divided by tree height) to height, where, again, the relationship is assumed constant and linear. Shelter or exposure effects are neglected. The term in parentheses is lumped into a single "blowdown" parameter (Table 1). The order of magnitude of this parameter is calibrated to provide slightly decreasing live biomass over time for old-growth stands, as has been observed in the Oregon Coast Range (T. Spies, U.S. Forest Service, personal communication, 2000). Following *Van Sickle and Gregory* [1990] and *Robison and Beschta* [1990], fall direction for each blowdown is chosen at random. Wood is distributed over the nodes on which the tree falls as if it were a perfect cone with the maximum tree height and D_{bh} calculated from equation (14), and biomass is conserved. In this way, wood is contributed to the channel from riparian zones and, depending on the tree height, may come from several nodes' distance. Fallen and deposited wood decay over time according to a single exponential with a rate derived for Douglas fir in western Oregon [*Harmon et al.*, 1986] (Table 1).

[45] Fires occur at exponentially distributed intervals and kill the entire forest, whereupon all trees fall. In nature, fires have variable size and intensity, and many trees are left standing, some alive, but, for simplicity, we assume we may neglect these variations. Neglecting size variation is justified by the finding that nearly all fires are larger than the basins we model (i.e., <5 km^2) [*Wimberly et al.*, 2000; M. Wimberly, U.S. Forest Service, personal communication, 2000]. As stand-killing fires typically burn only a small fraction of existing biomass, we assume that fires consume no wood [*Huff*, 1984; *Harmon et al.*, 1986; *Spies et al.*, 1988].

3.5. Initial Conditions

[46] Initial topography was generated from the DEM of the Hoffman Creek site and characteristics of the longitudinal channel profile sur⋯⋯ in the field. The DEM-based

valley topography presents problems for simulating debris flow runout because the DEM creates a longitudinal channel profile with large steps and intervening "flats" as long as several hundred meters such that debris flows tend to stop on the flats. The problem is exacerbated by the fact that we assume the initial channel profile to be bedrock and therefore not erodible. To remedy this problem we used characteristics of the longitudinal channel profile surveyed in the field to make a smooth initial bedrock profile.

[47] It is often observed that stream gradient, or slope, and contributing area are related as,

$$S = KA^{-\beta} \qquad (16)$$

where β is the concavity index; and K is the steepness index [*Flint*, 1974]. This relationship has been used in many studies to characterize streams [e.g., *Hack*, 1957; *Tarboton et al.*, 1991; *Willgoose*, 1994; *Moglen and Bras*, 1995; *Tucker and Bras*, 1998]. By finding contributing areas with the DEM and matching the longitudinal profiles from the DEM and field survey, we found the contributing area at every point along the surveyed profile. We then used the surveyed profile and the DEM contributing areas to derive K and β [*Lancaster et al.*, 2001]. We used the method of *Snyder et al.* [2000], in which the slopes are calculated between 10-m elevation intervals from the surveyed profile. To extrapolate a bedrock surface from the outlet up every branch of the network with equation (16), we "tuned" the steepness and concavity indexes to transition smoothly with the DEM elevations along the main channel (Table 1), though this method did result in steps along some tributary channels.

[48] In order to avoid an entrenched bedrock profile only one node wide, we repeatedly determined drainage directions according to a probabilistic criterion such that the probability of flowing to any downslope neighbor is proportional to the relative magnitude of the slope in that neighbor's direction, i.e., the probabilities are equal to the discharge fractions apportioned in a multiple flow direction scheme [*Moglen and Bras*, 1995] (whereas at all other times in the simulation flow direction is deterministic and follows steepest descent). The bedrock elevation was calculated for every channel node each time flow directions were redetermined, but node elevations were not changed until the end, when elevations at all nodes that had been channels, i.e., channel and valley nodes, were changed. This method resulted in some elevated bedrock "terraces" with thick soil adjacent to the channel (as noted for Figure 10). The profile-smoothing procedure successfully eliminated the main channel steps and flats that were artifacts of the DEM.

[49] Before the channel smoothing procedure, an initial soil layer evolved by diffusion and soil production over 6000 years [e.g., *Dietrich et al.*, 1995]. The storm model ran in isolation for 200 years to find the maximum intensity and duration during that time. Assuming a 6-year-old forest, when root strength is at a minimum, failure areas were determined for a storm with the maximum intensity and duration, and the soil was removed from these areas. In order to refill the hollows to different depths to mimic different times since failure, hillslope areas, i.e., channel source and channel-adjacent areas, were lumped into aggregates (Figure 3b), and evolution of the soil layer then proceeded for different random times between 0 and 2000

years in each aggregate. The forest at each failure site was regrown for the lesser of 300 years or the randomly chosen time of soil evolution to provide an old forest on all nodes except those that had recently failed. Finally, in order to remove unstable "banks" after channel smoothing, the landscape was subjected to a storm of average intensity and duration, and failed soil was removed from the system. This procedure produced a heterogeneous initial soil layer but did not completely prevent an influx of debris flows to the valley network due to larger storms near the beginning of the simulations.

4. Simulations and Field Methods

[50] The observed distribution of debris flow runout lengths provides both a basis for calibration of the model and context for the results. Because network structure, i.e., changes in slope and flow direction, may be a strong control on the distribution of runout lengths, we compare simulated and natural distributions for the same drainage basin, but we also compare our field data to that of other studies in nearby field areas in the Oregon Coast Range and to the prediction of the empirical model of *Benda and Cundy* [1990]. We also compared simulated and observed quantities of wood, both in debris flow deposits and small channels.

4.1. Debris Flows in the Study Area

[51] In the field we mapped all debris flow paths we could find in the entire channel network as defined by a 10^4 m^2-contributing area threshold. Where possible, we mapped these paths from source to deposit. This ground-based search utilized aerial photographs from as long ago as 1945 to help determine locations of failures and associated deposits. Horizontal runout lengths were determined by measuring path lengths on a DEM, although lengths measured in the field with a hip-chain provided a check on these measurements.

[52] Where possible, we measured total deposit and woody snout dimensions (Figure 1). In measuring these dimensions, we attempted to include volumes of sediment excavated by channel incision after deposition. With these dimensions, e.g., height, length, and width, and simplified representations of deposit geometry, e.g., triangular pyramid, trapezoidal prism, and wedge, we calculated total deposit and wood constituent volumes. In addition to the error associated with our measurements and geometric simplifications, void spaces in both wood and sediment masses were included in the respective constituent volumes. Voids in piles of wood might be filled with air, sediment, and/or water. Voids in sediment deposits might be filled with air and/or water. Also, wood that might be buried within sediment deposits would be counted as part of the sediment constituent. It is unclear how these various errors might affect calculated wood fractions. In order to provide a comparison between simulated and actual wood quantities encountered by debris flows, we also measured down wood volumes in small channels according to the method of *Harmon et al.* [1986] and *Harmon and Sexton* [1996].

4.2. Simulations

[53] To explore the strengths of the hypothesized effects of wood on debris flows, we simulated many events over 300 years in a drainage basin with evolving valley topography and a single fire   82 years. All simulations

include the effect of root strength on landslide initiation (equation 2) and scour (equation 8). Simulations included both, one, or none of the wood effects, as explained below.

[54] 1. For wood entrainment and decreased velocity at bends (WB), wood is entrained and incorporated as a debris flow constituent and thereby reduces debris flow velocity according to equation (4). Wood at failure sites, standing and fallen, and wood in runout paths, standing, fallen, and deposited, are incorporated by debris flows such that they denude their paths of live vegetation and fallen debris and may scour deposited wood. Debris flow velocity decreases at bends according to equation (12). Because it should best represent current conditions in the study area and we want to simulate possible changes resulting from wood removal, this case is used to calibrate the debris flow runout model. Simulations with unelevated, hydrostatic basal pore pressure, p_b, in equation (4) have debris flow runout lengths that are, in general, shorter than those observed. Higher pore pressures result in lower friction according to equation (4) and therefore longer simulated runout lengths. As suggested by the results of *Iverson et al.* [1997] and *Reid et al.* [1997] and the method of *Denlinger and Iverson* [2001], we began our calibration procedure by multiplying hydrostatic pressure by 1.8 to get the basal pore pressure in equation (4) and running several simulations with different stochastic storm sequences. This value for the pore pressure multiplier satisfactorily reproduced the observed distribution so further variation of this factor in order to obtain a satisfactory fit to the data was not necessary. We note, however, that simultaneous calibration to the field and the flume is not possible for this model, i.e., when this result is applied to a case imitating experiments at the USGS Debris Flow Flume, runout lengths are much longer than those observed experimentally (R. Iverson, USGS Cascades Volcano Observatory, personal communication, 2002).

[55] 2. For no wood entrainment (NW), debris flows do not entrain wood. Bends do decrease debris flow velocity according to equation (12).

[56] 3. For no effect of bends on velocity NB, bends do not decrease debris flow velocity. Debris flows do entrain wood, which reduces velocity according to equation (4).

[57] 4. For no wood entrainment and no effect of bends on velocity (NWB), debris flows do not entrain wood, and bends do not reduce debris flow velocity.

5. Results

5.1. Field Observations of Debris Flows in the Study Area

[58] We found 38 debris flow paths in the Hoffman Creek study area and were able to identify both initiation and deposition sites and thus determine runout lengths for 28 of the 38 debris flows mapped (Figures 5, 6, and 7 and Table 2); age ranges were determined for all of the events from aerial photographs. Note that while many debris flows stopped at large-angle bends, other debris flows continued through bends with as large or larger angles. For example, debris flows 3 and 4 started at nearly the same location at different times. The former (earlier) stopped at the first large bend, but the latter (later) continued through that same large bend and the next (Figure 5). These results support our use of equation (12) and confirm our earlier assertion that while the effect of bend angles on runout is strong, no threshold
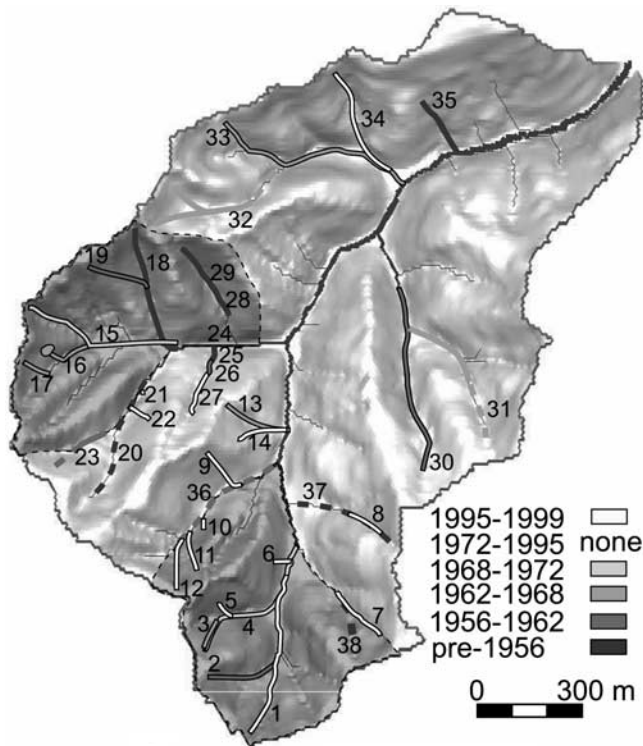
Figure 5. Shaded relief map of the Hoffman Creek study area with mapped debris flows. The more darkly shaded areas of the map with a dashed outline indicate areas harvested circa 1965. Mapped debris flow tracks are numbered according to Table 2 and shaded according to age, and those tracks representing debris flows with known runout length are outlined in black to improve visibility. Dashed, unoutlined debris flow tracks indicate debris flows with distinct deposits but unknown sources or, conversely, known sources but unknown termini.

Figure 6. Cumulative distribution functions of debris flow runout lengths from the Hoffman Creek study area (present study), the "Mapleton" area of the Oregon Department of Forestry's (ODF) study of debris flows occurring during February 1996 [*Robison et al.*, 1999], and the Knowles Creek study area of *Benda and Cundy* [1990].

angle exists, and other factors, such as bend-entering velocities, amounts of entrainable material, and valley slopes, help determine whether particular debris flows will continue through or stop at particular bends.

[59] Relative to the real, long-term distribution, we expect our sample distribution (Figures 6 and 7) is biased in two ways. First, we probably missed some smaller, more frequent events with shorter runout lengths during the approximately 50-year span of the mapped debris flows because evidence of these small events is more likely to be obliterated by later events, and smaller events are more difficult to find. Second, we probably missed the longest, least frequent runout events likely to occur over several centuries because of the relatively short time represented by the mapped events.

[60] Data from the Knowles Creek study area of *Benda and Cundy* [1990] and the Mapleton study area of *Robison et al.* [1999] provide useful comparisons of our data to other data from nearby, similar areas (Figure 6). Our survey was similar to that of *Robison et al.* [1999] in that both attempted to locate every debris flow in the study area with a ground-based survey. This similarity explains the relative similarity of the debris flow runout length distributions from our data and theirs. Their study was different in that they only mapped debris flo   at occurred during February,
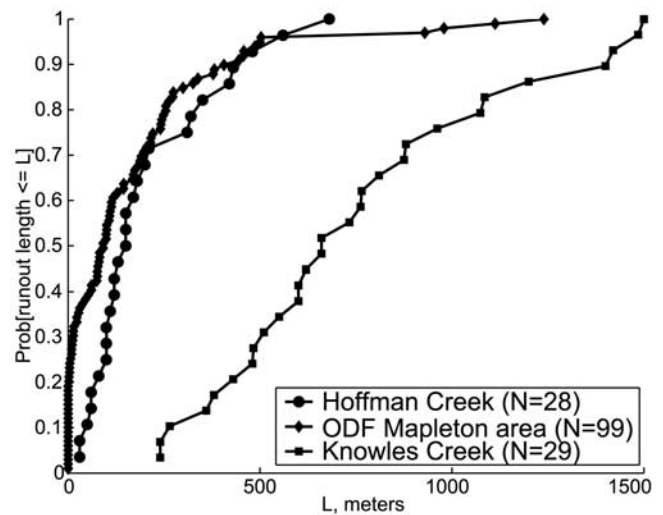
1996, while we mapped all debris flows regardless of age. Unlike our survey, theirs included all failures with a detectable scarp, no matter how small, even small stream bank collapses, and resulted in many "debris flows" of zero runout length. Examination of their data revealed that all but a few of the lengths less than 30 m were for "channel adjacent" failures (Oregon Department of Forestry, unpublished data, 1999), so this different criterion explains the difference between our distribution and theirs at short runout lengths. Finally, their study area was a rectangular area chosen because of the high areal density of landslides observed during preliminary aerial reconnaissance. That
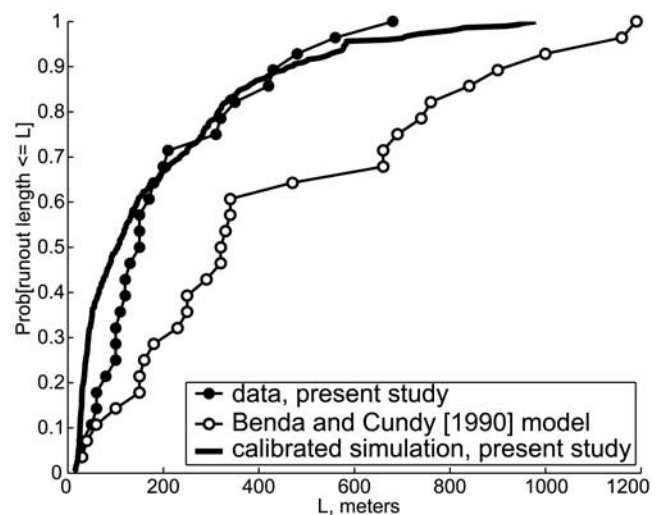

Figure 7. Comparison of cumulative distribution functions of debris flow runout lengths measured in the Hoffman Creek study area, predicted by the model of *Benda and Cundy* [1990], and simulated by the calibrated model with wood effects from the present study.

Table 2. Debris Flows Mapped in Hoffman Creek Study Area

Debris Flow	Runout Length, m	Predicted Runout Length,[a] m	Total Deposit Volume, m³	Wood Fraction, %	Time Range of Occurrence
1	430	1,190	2500	74	1995–1999
2	210	1,160	no data	no data	1956–1962
3	120	250	no data	no data	1962–1968
4	480	250	no data	no data	1968–1972
5	30	160	35	37	1995–1999
6	60	60	110	43	1995–1999
7	120	1000	no data	no data	1995–1999
8	130	290	33	44	1995–1999
9	110	660	480	76	1995–1999
10	50	660	50	90	1995–1999
11	80	840	170	61	1995–1999
12	100	900	370	57	1995–1999
13	180	180	no data	no data	1962–1968
14	150	150	495	34	1995–1999
15	420	740	no data	no data	1968–1972
16	170	40	290	46	1962–1968
17	60	760	no data	no data	1962–1968
18	350	320	no data	no data	<1956
19	150	320	61	70	1956–1962
20	unknown	N/A	1000	71	<1956
21	30	30	no data	no data	1995–1999
22	100	100	94	41	1995–1999
23	unknown	N/A	560	92	1956–1962
24	unknown	N/A	no data	no data	<1956
25	unknown	N/A	no data	no data	<1956
26	300	340	no data	no data	1956–1962
27	100	340	no data	no data	1995–1999
28	unknown	N/A	no data	no data	<1956
29	200	330	no data	no data	<1956
30	560	690	no data	no data	1956–1962
31	unknown	N/A	no data	no data	1962–1968
32	unknown	N/A	no data	no data	1962–1968
33	680	470	no data	no data	1962–1968
34	310	230	no data	no data	1995–2000
35	150	150	no data	no data	<1956
36	unknown	N/A	no data	no data	1956–1962
37	unknown	N/A	no data	no data	<1956
38	unknown	N/A	no data	no data	<1956
Mean[b]	209	450	450	60	N/A

[a]Runout lengths predicted by the model of *Benda and Cundy* [1990].
[b]"Unknown" or "no data" excluded from calculation of mean.

area (22 km²) was much larger than our study area (2.1 km²), the number of debris flows mapped was larger, and therefore the probability of finding larger, rarer events was greater. These differences in area and number, then, probably explain the difference between our distribution and theirs at longer runout lengths. *Benda and Cundy* [1990] do not specify how debris flows were selected for inclusion in their data set. The shortest of these debris flow runout lengths is longer than 75% and 72% of the lengths in *Robison et al.*'s [1999] and our data sets, respectively, and 13% and 48% of the *Benda and Cundy* [1990] lengths are longer than the longest of the lengths in *Robison et al.*'s [1999] and our data sets, respectively. Their study area was the entire Knowles Creek basin (52 km²), so it was likely to include more long runout lengths than the other two study areas. Also, that basin has been intensively logged for the last fifty years [*Benda and Cundy*, 1990], and debris flows there probably contain less wood than those in, e.g., our study area. As we will show, less wood may lead to longer runout lengths. The *Benda and Cundy* [1990] data set has the lowest areal density of debris flows of the three studies (0.56 km⁻² for *Benda an   dy* [1990] versus 4.5 km⁻²

for *Robison et al.* [1999] and 13 km⁻² for the present study), which suggests that the *Benda and Cundy* [1990] data are biased toward larger debris flows.

[61] Given these differences between our data and that of *Benda and Cundy* [1990], it is not surprising that their model, calibrated with their data, predicts generally longer-than-observed runout lengths in the Hoffman Creek study area (Figure 7 and Table 2). Although some runout lengths are underpredicted or predicted correctly, most of the runout lengths are overpredicted (Table 2). Although both the observed and predicted distributions are approximately exponential in shape (Figure 7), the distribution predicted by the *Benda and Cundy* [1990] model has a mean runout length more than twice as long as that of the field data (Table 2).

[62] We were able to measure deposit volume and wood fraction for 14 of the 38 debris flows mapped in our study (Table 2). For these measured deposits the average wood fraction, i.e., the ratio of wood to total deposit volume, was 0.60, and the standard deviation was 0.19. Neglecting the possible errors previously noted, the observed ratios may, on the one hand, be underestimates of actual wood fractions because (1) some wood has likely decayed and/or been moved downstream, e.g., by later debris flows and (2) some sediment has likely been added to deposits by fluvial deposition. On the other hand, the measurements could neglect debris flow deposits with little or no wood because such deposits may not be preserved behind wood dams. All of the most recent debris flows mapped in the field cleared all wood from their paths. In the field, we measured wood volumes as great as 0.54 m³/m² in small channels that had not been recently scoured by debris flows.

5.2. Simulations

[63] The calibrated runout length distribution for the case with both wood entrainment and decreased velocity at bends (WB) closely resembles the observed distribution (Figure 7), and a distribution including the debris flows from this simulation plus those from four more calibration runs could not be rejected, even at the 10% level, as a model for the observed distribution with a Kolmogorov-Smirnov test [*Benjamin and Cornell*, 1970]. The differences between the simulated and observed distributions actually reflect the expected biases of the data. The simulated distribution has more short runout lengths, and the longest runout lengths are longer than the longest of those measured in the field. The differences between the simulated and observed distributions also resemble the differences between our observed distribution and that of *Robison et al.* [1999] (Figure 6); that is, our simulated and *Robison et al.*'s [1999] observed distributions are similar. Although it does not necessarily follow that our simulation results would be as similar to the *Robison et al.* [1999] data if the model were applied to their study area, that apparent similarity does at least indicate that our calibrated model produces results that are typical of this part of the Oregon Coast Range.

[64] Removing wood entrainment and its effect on debris flow velocity greatly increased runout lengths in part of the distribution, especially for the longest, but left essentially unchanged the shortest ~30% of runout lengths (Figure 8). Debris flows that travel further have greater wood entrainment and therefore greater effect of that entrainment on runout length. Both the mean and maximum runout lengths
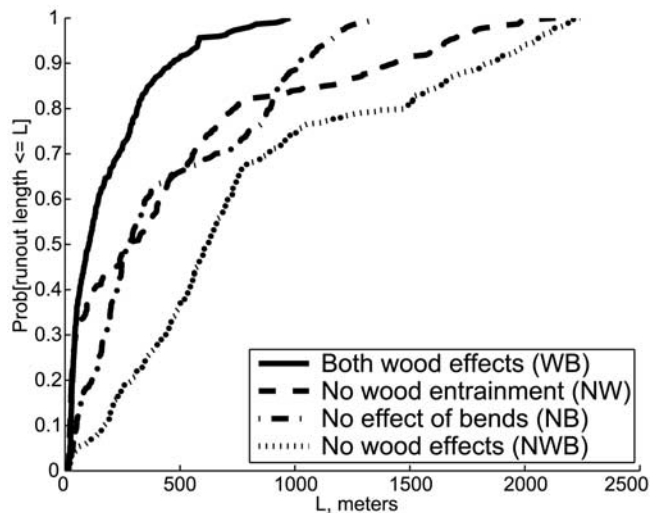
Figure 8. Cumulative runout length distributions for the model simulations: case with both effects of wood, entrainment and decreased velocity at bends (WB); case with no wood entrainment (NW); case with no effect of bends on velocity (NB); and case with neither wood entrainment nor effect of bends on velocity (NWB) (Table 3).

in this case (NW) increased by more than 100% (Table 3) over the first (WB) case. The shortest runout lengths were apparently unaffected by removing only wood entrainment and instead had their runout halted by sharp bends soon after initiation, similar to what we observed in the field, where most debris flows with short runout lengths stopped at large-angle bends (Table 2 and Figure 5). This larger effect of bends on shorter runout lengths is illustrated by the effect of removing the dependence of debris flow velocity on bends (NB). In the NB simulation, the maximum runout length did not increase much beyond the range of variability we observed in the several calibration runs of the WB case, but the mean runout length increased by more than 100% (Table 3), and even the shortest runout lengths were increased (Figure 8). It is evident from the NB simulation that debris flows that travel farther experience relatively little effect of bends, i.e., though they may have stopped at bends in the WB simulation they would have stopped soon had they not encountered those bends. Similarly, in the study area, although 5 of the 10 longest runout lengths terminated at bends, 3 of those 5 termini are in close proximity to termini of others of the 10 longest runout lengths in straight reaches (Table 2 and Figure 5). Removing both the effects of wood entrainment and bends on debris flow velocity, then, increases runout lengths throughout the distribution (NWB, Figure 8). The maximum length is not increased appreciably over the case with only wood

entrainment removed (NW), but all runout lengths are significantly increased over the case with only the effect of bends removed (NB), and the mean runout length is increased by more than 400% over the first case with both wood effects (WB). Evidently, once the effect of bends is removed, wood entrainment affects all debris flows, even the shorter ones, and emerges as a dominant control on runout length.

[65] Note that our simulation with "both" hypothesized effects of wood may not include some effects of wood and trees that may be important in the field, such as resistance to breaking and uprooting by large logs and trees. If these effects are indeed important, then our simulations may actually underestimate the effect on debris flow runout lengths of removing wood and trees from the system. That is, our simulations may represent a conservative estimate of the impact of removing wood.

[66] Comparison of simulation results with field data indicates that the magnitude of the simulated momentum loss due to wood entrainment is reasonable. In the simulation with both wood effects (WB), the fraction of wood in debris flows, i.e., the ratio of wood volume to the sum of wood and bulk sediment (assuming alluvial porosity, Table 1) volumes, just before the beginning of deposition (i.e., before any refailure of deposits) averaged 0.269 with a standard deviation of 0.354. This low average wood fraction is partly due to the fact that more than 40% of the simulated debris flows had negligible wood volume due to combined effects of landslides initiating at sites with almost no wood traveling as debris flows down channels cleared of wood by previous debris flows. In effect, these debris flows are similar to the more fluid debris flow tails that follow woody snouts in the field, although unlike in the field, these tails do not have the effect of pushing those woody snouts along, hence our need to elevate pore pressures in the runout model. Rather, these fluid tails in the model pile up behind previous, woody debris flow deposits. It is illustrative, then, to consider only those debris flows with a significant amount of wood, say >1%. For these woody debris flows the ratio of wood to bulk deposit volume averages 0.512 with a standard deviation of 0.338. This estimate is still somewhat smaller than the average observed wood fraction of 0.60 (Table 2) but is similar, especially given the suspected errors and biases in these measurements, as discussed above. It is also useful in assessing the modeled effect of wood entrainment to compare average wood volumes in the entire simulation domain with wood volumes measured in small channels without recent debris flow tracks. In all simulations, areally averaged volumes of woody debris following fires were in the range of $0.5-0.7$ m^3/m^2. Simulated wood volumes were therefore similar to those measured in the field, although the upper end of the range is larger than any volume measured in the field.

Table 3. Model Simulations

Case	Number of Debris Flows	Average Landslide Volume, m^3	Mean Runout Length, m	Maximum Runout Length, m	Number of Fires
Wood entrainment and bends (WB)	297	118	185	980	1
No wood entrainment (NW)	379	112	468	2130	1
No bends (NB)	324	112	442	1350	1
No wood entrainment or bends NWB)	359	111	791	2240	1

Table 4. Summary of the Present Study and Landslide and Debris Flow Studies in Areas Geologically Similar to the Hoffman Creek Site in the Oregon Coast Range

Average Landslide Volume, m³	Number	Period of Record, years	Reference
610	73	single storm	*May* [1998]
450	36	N/A	*Benda and Cundy* [1990]
54	39	15	*Swanson et al.* [1977][a]
110	317	10	*Swanson et al.* [1977][b]
250	35	10	*Montgomery et al.* [2000]
20	92	single storm	*Robison et al.* [1999][c]
115	76	single storm	*Robison et al.* [1999][d]
113	340	300	simulations, present study[e]

[a]Field-based survey in mature forest.
[b]Air photo-based survey in recent clear-cut.
[c]Landslide initiation site only, Mapleton site only.
[d]Landslide and nonchannelized debris flow, Mapleton site only.
[e]Average values for four simulations, WB, NW, NB, and NWB.

Average simulated debris flow volume is within the range of values reported by other studies (Tables 3 and 4), but that range is large, and our simulated values are at the lower end of the reported range. It appears, then, that the relative effect of wood is reasonable but difficult to compare precisely with field data.

[67] The effect of wood on runout lengths has implications for both sediment output from and depositional patterns within the basin. In the simulations with both wood effects and neither wood effect (WB and NWB, respectively), sediment output for each is dominated by step-increases due to debris flows reaching the outlet, but output in the case with wood effects is much smaller than in the case without wood effects, a result that indicates that far fewer debris flows reached the outlet in the case with wood (Figure 9). In the WB simulation cumulative sediment output was dominated by a pulse due to a few debris flows reaching the outlet early in the simulation (Figure 9a). The major contributor to sediment output after that early pulse was a much smaller pulse following the fire, also due to debris flows reaching the outlet, and the latter pulse is similar in magnitude to subsequent output due to fluvial transport. In the NWB simulation cumulative sediment output was dominated by large pulses of similar magnitude due to debris flows reaching the outlet both early in the simulation and after the fire (Figure 9b). Output due to fluvial transport is insignificant relative to the magnitudes of either of the pulses and is, in fact, not detectable on the graph. The total cumulative sediment output for the NWB simulation was nearly an order of magnitude larger than the output for the WB simulation. For these simulations of the study area, then, removing wood from the system dramatically changed both the amount of, and the processes significantly contributing to, sediment output.

[68] Wood removal also changed the distribution of deposits within the basin's valley network. In the WB simulation, wood entrainment, sharp bends, and low valley slopes all act to halt debris flows, and large deposits are distributed at several locations in the basin (Figure 10a). In the NWB simulation, low valley slopes are the main thing halting debris flows, and large deposits are concentrated in a single reach near the basin outlet (Figure 10b). Of the two simulated depositional pa   , the deposits of the WB

simulation more closely resemble the field data. As in the WB simulation, debris flow deposits in the field are widely distributed throughout the basin, even in the uppermost reaches of the channel network (Figure 5).

6. Discussion

[69] The results indicate that wood in the Oregon Coast Range and, by extension, much of the Pacific Northwest is an important debris flow constituent that acts as a first order control on not only runout lengths but also locations of deposition in the network. A corollary result is that removal of wood from small drainage basins such as the study area would increase runout lengths enough to significantly increase the downstream extent of direct impact by debris flows. These results are robust because they depend only on the relatively simple physics of conservation of momentum and the widely recognized effect of bends [e.g., *Benda and Cundy*, 1990; *Robison et al.*, 1999].

[70] Velocity reduction associated with bulldozing and scouring wood and trees along the runout path had a large effect on simulated runout length distributions. Our physical arguments for this wood effect are based on conservation of momentum, but in highly simplified form. Debris flows are, of course, not rigid blocks, and loss of debris flow velocity through acceleration of wood may not be as simple as in our model, particularly because of the flushing and pushing effects of debris flow head-tail interactions. Large clasts and wood tend to become jammed up at the fronts of debris flows and, as a result, to increase resistance there [*Iverson and Denlinger*, 2001]. This increase in resistance accentuates the interaction between head and tail: when the head slows down the more fluid tail catches up, the flow depth increases, and that increased depth and the transfer of momentum from the tail to the head both flushes it out and pushes it along. In the model, this flushing and pushing effect is absent, so simulated debris flows may not travel as far as in the field, all else being equal. Our elevation of pore
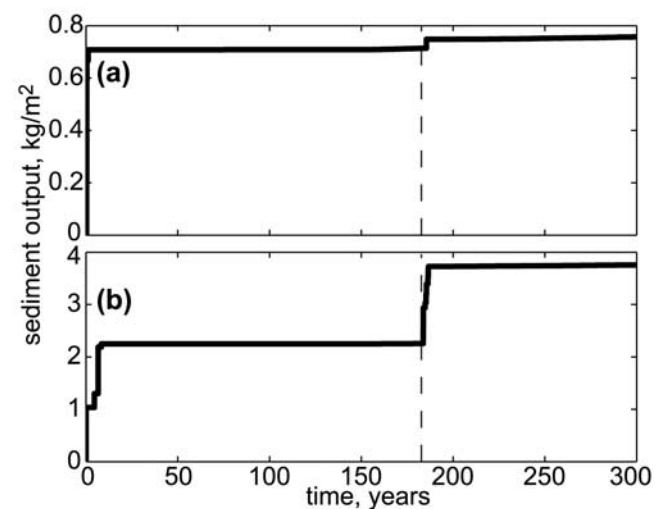

Figure 9. Cumulative sediment output (solid lines) and times of fire occurrence (dashed lines) for simulation cases with (a) both wood effects (WB) and (b) no wood effects (NWB). Note that the vertical axes of Figures 9a and 9b are different.
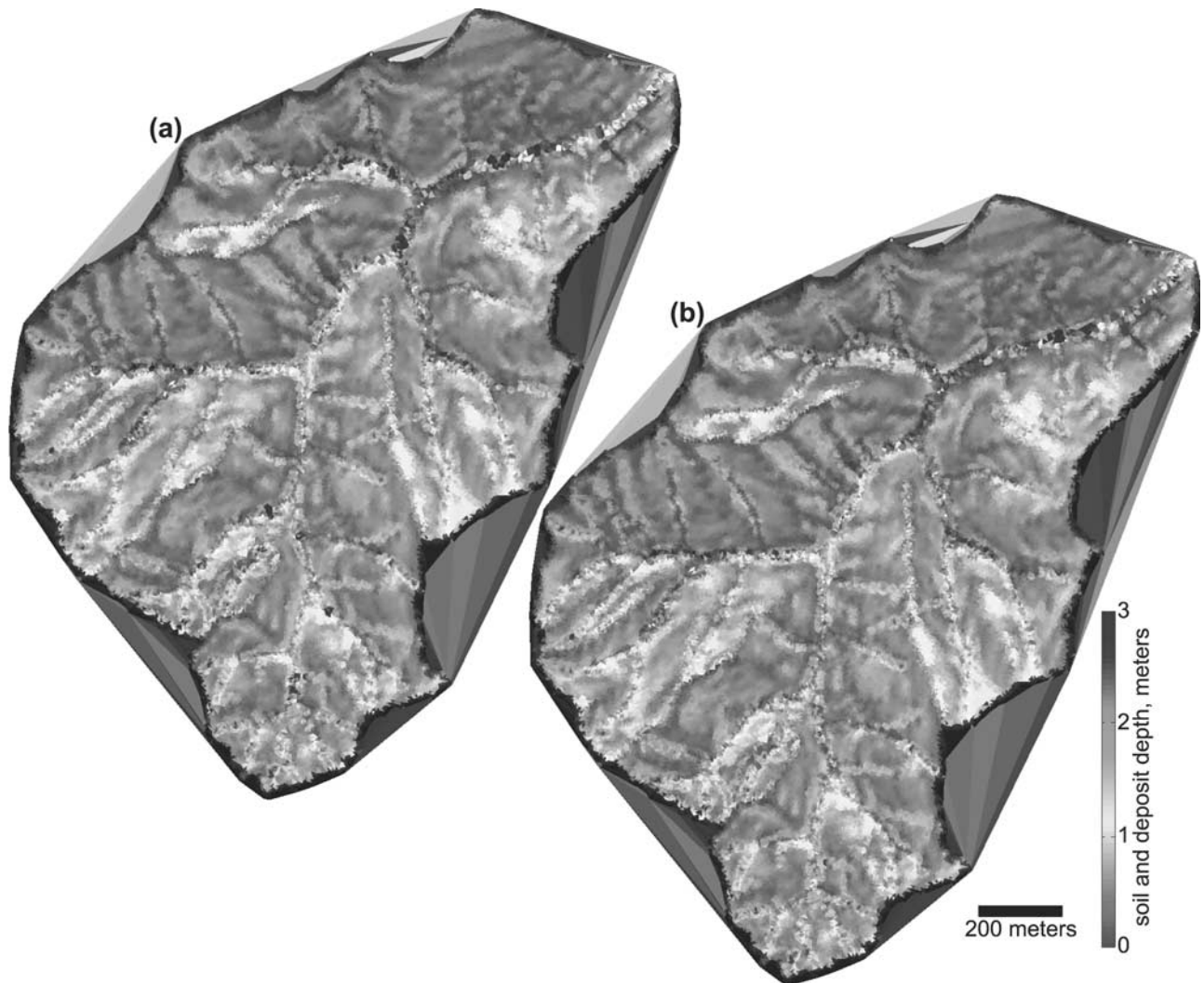
Figure 10. Shaded relief maps colored according to simulated soil, sediment, and wood deposit depth at 200 years (18 years after the fire) for simulation cases (a) with both wood effects (WB) and (b) without either wood effect (NWB). The color scale is compressed to highlight deposits thicker than 3 m, which appear as dark blue patches. Note that the blue channel-side deposits found in both simulations are mainly thick soil accumulations at the bottoms of hillslopes, i.e., remnants of flat valley bottoms that are not affected by the channel-smoothing procedure during initialization. See color version of this figure at back of this issue.

pressures in the model is some compensation for this effect. That said, we have some confidence in the tendency and rough magnitude of the modeled effect of wood entrainment because it does have a physical basis, and simulated and observed wood quantities are similar. Wood quantities are slightly higher in the simulation than in small channels in the study area. It is possible that the wood quantities in the model are realistic but simply more representative of postfire conditions than postharvest or mature forest conditions, such as in the study area. In any case, this difference might indicate that the simulated increase in runout lengths with wood removal might be slightly greater than would actually occur if wood were removed from the Hoffman Creek study area.

[71] It is widely recognized that debris flow runout is strongly affected by bends, especially those at tributary junctions [e.g., *Benda and Cundy*, 1990], but the true form of that effect is unkno   account for this effect, we introduced a rule (equation 12) that is consistent with our observations but has limited physical justification: we essentially assume that wood makes debris flows act like nonfluid objects that are constrained to follow the downstream direction after colliding with the valley walls. This particular physical assumption, though self-consistent, is relatively arbitrary as it is based only on observations of debris flow deposits and runout tracks and not on observations of actual debris flows in motion. Such observations are necessary to better understand the effect of wood on the motion of debris flows through bends. Therefore flume experiments incorporating large volume fractions of large wood pieces in debris flows moving through bends should be a top experimental priority.

[72] An important result of this study is that debris flows' constituents, e.g., wood content, have a first-order effect on runout lengths that is significant even in the context of the strong effect of bends in the channel network, which we

assume is also attributable to wood, and other network effects such as changes in valley slope and width. This finding has important implications for management because it is now common practice to assess the risk of debris flow inundation for a stream reach based on debris flow runout models, such as that by *Benda and Cundy* [1990], where flows stop according to slope and direction angle change criteria that are calibrated from debris flow runout data. Such data are, of course, representative of current conditions at the data collection site and necessarily reflect any biases inherent in that data collection. So, although such models may be adequate predictors now, our results indicate that if there are large changes in conditions affecting debris flow runout, such as wood and sediment volumes in potential runout paths, then calibrated, empirical models would need to be modified or recalibrated in order to adequately predict risk following such large changes. Current forestry practices that prescribe harvest every 40–50 years could represent such a change because, as old, "legacy" wood decays, forests are too young to contribute substantial new wood to hillslopes, valleys, and channels.

[73] The fact that the calibrated model mimics the observed distribution for not only our study area but also *Robison et al.*'s [1999] Mapleton area gives us some confidence in applying the model to other locations. It is possible, however, that differences in network structure could have significant effects and would lead to poor performance in other basins.

[74] Differences in network structure do not appear to be responsible for the discrepancy between our data and that of *Benda and Cundy* [1990] because their model, which was calibrated with their data, generally overpredicts runout lengths in the Hoffman Creek study area. Rather, the discrepancy between observations and the overprediction by their model indicate the necessity of recalibration of the *Benda and Cundy* [1990] model if it is to realistically represent runout lengths for an unbiased sample of debris flows. Their original calibration data were collected in a relatively wood-poor area, but that wood poorness is only relative: we have observed large quantities of wood in debris flow deposits in their study area. These facts (overprediction by their model and only relatively low wood volumes in their study area) indicate that the eventual effects of logging, once existing wood has decayed, could be much greater than those realized so far.

[75] The distribution of runout lengths has a strong effect on locations of sediment storage in valleys such as in the study area [*Lancaster et al.*, 2001]. Locations of sediment and wood storage, in turn, strongly affect debris flow runout and deposition. Previous deposits change local slopes and flatten and widen valley bottoms, and they provide material for entrainment. The effect of previous deposits is evident in the sediment output for the calibrated WB simulation. The smooth initial channel allowed a relatively large early pulse of debris flows to reach the basin outlet. Subsequent debris flow deposition created barriers to runout and, after the fire, restricted debris flows reaching the outlet to a much smaller pulse and allowed for a relatively large output by fluvial sediment transport.

[76] This significance of fluvial transport later in the simulation and the role of wood in enhancing that significance are consistent with the results of previous studies.

Benda [1990] found that debris flows traveled through first- to third-order channels (the study area is a fourth-order basin according to our channel head criterion) and that deposition in higher-order channels and valleys was mainly at the mouths of first- and second-order channels. *Swanson and Lienkaemper* [1978] observed that wood in streams increases storage capacity and thus buffers downstream reaches from sediment input pulses, and recent studies have confirmed this result [e.g., *Massong and Montgomery*, 2000; *Lancaster et al.*, 2001]. Of course, streams larger than fourth-order do receive sediment pulses from debris flows, but from relatively small tributaries. Our results imply that removing wood would increase runout lengths enough that larger tributaries, e.g., fourth-order, could start contributing debris flows directly to larger streams. For example, we found no evidence of past debris flow deposits at the mouth of the study basin, but our results indicate that if the basin were stripped of wood, then this basin might become a significant source of debris flow input to the main stem of Hoffman Creek.

[77] Such regime changes, i.e., from fluvial- to debris flow-dominated sediment output, could affect aquatic habitat. It is already recognized that wood, by increasing local gravel retention and providing structure for habitat elements, is a key contributor to spawning and rearing habitat for salmonid species [e.g., *Lisle*, 1986; *Bisson et al.*, 1987; *Reeves et al.*, 1993; *Montgomery et al.*, 1995; *Beechie and Sibley*, 1997; *Martin*, 2001], especially in smaller streams such as in our study area [*Bilby and Ward*, 1989]. Our results imply that wood is also an important control on the dominant process regimes of sediment deposition in and export from stream reaches and thus affects the total lengths of streams dominated by debris flow and fluvial processes, respectively. Future research should include better quantification of the effects of not only wood on dominant sediment output regime but also output regime on aquatic habitat because our results suggest a strong coupling among forest dynamics, mass movement processes, and channel morphology.

7. Conclusion

[78] The model results show that two proposed mechanisms by which wood reduces debris flow runout velocity each have potentially large effects on debris flow runout lengths. We proposed that (1) entrainment of wood by debris flows reduces velocity because momentum conservation requires that addition of wood mass be compensated by a loss in velocity and (2) flow direction angle changes (bends) reduce velocity because wood causes debris flows to behave more like objects colliding with valley walls than like a fluid that flows between them. Simulated removal of these two effects, both singly and in combination, resulted in significant shifts of runout length distributions toward longer lengths. Removing wood entrainment had the greatest effect on longer runout lengths because longer debris flows would otherwise entrain the most wood. Removing velocity reduction at bends had the greatest effect on shorter runout lengths because those debris flows would otherwise stop at sharp bends shortly after initiation. Removing both wood effects greatly increased all runout lengths: the maximum and mean lengths increased by over 100% and over 400%, respectively.

[79] Longer runout lengths due to the removal of wood effects resulted in more debris flows reaching the outlet and thus greater total sediment output and insignificant contribution to that total by fluvial transport. In addition to simply increasing runout lengths, the removal of the wood effects left valley slope as the only first-order control on debris flow runout. As a result, debris flow deposits were concentrated at, essentially, one location near the basin outlet. Debris flows subject to the multiple controls of wood entrainment, bends in the channel network, and valley slope deposited in multiple locations throughout the basin. This wider distribution of deposits is more similar to the distribution of deposits mapped in the field.

[80] The calibrated distribution of runout lengths was similar to observed distributions in both our study area and *Robison et al.*'s [1999] nearby Mapleton area, and these observed distributions were similar to each other. On the basis of these facts we speculate that our field and modeling results are typical for this part of the Oregon Coast Range.

[81] Our proposed wood effects are based on simple physics and observations [e.g., *Benda and Cundy*, 1990], and simulated wood volumes are similar to those observed. While we do not claim to have accounted for every significant effect of wood, we believe that the effects we have modeled are robust. Our results indicate that the effects of wood removal on debris flow runout lengths, deposition patterns, and sediment output regimes in the Oregon Coast Range are large. If our simulations have not correctly estimated the magnitudes of these effects, it is likely that our results underestimate the actual magnitudes.

References

Beechie, T. J., and T. H. Sibley, Relationships between channel characteristics, woody debris, and fish habitat in northwestern Washington streams, *Trans. Am. Fish. Soc.*, *126*(2), 217–229, 1997.

Benda, L. E., The influence of debris flows on channels and valley floors in the Oregon Coast Range, USA, *Earth Surf. Processes Landforms*, *15*(5), 457–466, 1990.

Benda, L. E., and T. W. Cundy, Predicting deposition of debris flows in mountain channels, *Can. Geotech. J.*, *27*(4), 409–417, 1990.

Benda, L., and T. Dunne, Stochastic forcing of sediment supply to channel networks from landsliding and debris flow, *Water Resour. Res.*, *33*(12), 2849–2863, 1997.

Benjamin, J. R., and C. A. Cornell, *Probability, Statistics, and Decision for Civil Engineers*, 683 pp., McGraw-Hill, New York, 1970.

Bilby, R. E., and J. W. Ward, Changes in characteristics and function of woody debris with increasing size of streams in western Washington, *Trans. Am. Fish. Soc.*, *118*(4), 368–378, 1989.

Bisson, P. A., R. E. Bilby, M. D. Bryant, C. A. Dolloff, G. B. Grette, R. A. House, M. L. Murphy, K. V. Koski, and J. R. Sedell, Large woody debris in forested streams in the Pacific Northwest: Past, present, and future, in *Streamside Management: Forestry and Fishery Interactions, Contrib. 57*,
edited by E. O. Salo and T. W. Cundy. pp. 143–190, Univ. of Wash. Inst. of For. Resour., Seattle, 1987.

Burroughs, E. R., Landslide hazard rating for portions of the Oregon Coast Range, paper presented at Symposium on Effects of Forest Land Use on Erosion and Slope Stability, East-West Cent., Univ. of Hawaii, Honolulu, 1984.

Burroughs, E. R., and B. R. Thomas, Declining root strength in Douglas fir after felling as a factor in slope stability, *USDA For. Serv. Res. Pap., INT-190*, 27 pp., 1977.

Denlinger, R. P., and R. M. Iverson, Flow of variably fluidized granular masses across three-dimensional terrain: 2. Numerical predictions and experimental tests, *J. Geophys. Res.*, *106*(B1), 553–566, 2001.

Dietrich, W. E., and T. Dunne, Sediment budget for a small catchment in mountainous terrain, *Z. Geomorphol.*, *29*, 191–206, 1978.

Dietrich, W. E., R. Reiss, M.-L. Hsu, and D. R. Montgomery, A process-based model for colluvial soil depth and shallow landsliding using digital elevation data, *Hydrol. Processes*, *9*, 383–400, 1995.

Du, C., An algorithm for automatic Delaunay triangulation of arbitrary planar domains, *Adv. Eng. Software*, *27*(1–2), 21–26, 1996.

Duan, J., A coupled hydrologic-geomorphic model for evaluating effects of vegetation change on watersheds, Ph.D. thesis, 133 pp., Oreg. State Univ., Corvallis, 1996.

Duan, J., J. Selker, and G. E. Grant, Evaluation of probability density functions in precipitation models for the Pacific Northwest, *J. Am. Water Resour. Assoc.*, *34*(3), 617–627, 1998.

Eagleson, P. S., Climate, soil, and vegetation: 2. The distribution of annual precipitation derived from observed storm sequences, *Water Resour. Res.*, *14*(5), 713–721, 1978.

Engelund, F., and E. Hansen, *A Monograph on Sediment Transport in Alluvial Streams*, 3rd rev. ed., 62 pp., Teknisk Forlag, Copenhagen, 1972.

Flint, J. J., Stream gradient as a function of order, magnitude, and discharge, *Water Resour. Res.*, *10*, 969–973, 1974.

Forest Ecosystem Management Assessment Team (FEMAT), *Forest Ecosystem Management: An Ecological, Economic, and Social Assessment*, 1056 pp., U. S. Gov. Print. Off., Washington, D. C., 1993.

Garde, R. J., and K. G. Ranga Raju, *Mechanics of Sediment Transportation and Alluvial Stream Problems*, 2nd ed., 618 pp., John Wiley, New York, 1985.

Garman, S. L., S. A. Acker, J. L. Ohmann, and T. A. Spies, Asymptotic height-diameter equations for twenty-four tree species in western Oregon, *Res. Contrib. 10*, 22 pp., For. Res. Lab., Oregon State Univ., Corvallis, 1995.

Govers, G., Evaluation of transporting capacity formulae for overland flow, in *Overland Flow*, edited by A. J. Parsons and A. D. Abrahams, pp. 243–273, Chapman and Hall, New York, 1992.

Grier, C. C., and R. S. Logan, Old-growth *Pseudotsuga menziesii* communities of a western Oregon watershed: Biomass distribution and production budgets, *Ecol. Monogr.*, *47*, 373–400, 1977.

Hack, J. T., Studies of longitudinal stream profiles in Virginia and Maryland, *U. S. Geol. Surv. Prof. Pap.*, *294-B*, 97 pp., 1957.

Haff, P. K., Limitations on predictive modeling in geomorphology, in *The Scientific Nature of Geomorphology*, edited by B. L. Rhoads and C. E. Thorn. pp. 337–358, John Wiley, New York, 1996.

Hammond, C., D. Hall, S. Miller, and P. Swetik, Level 1 stability analysis (LISA), documentation of version 2.0, *USDA For. Serv. Gen. Tech. Rep., INT-285*, 190 pp., 1992.

Harmon, M. E., et al., Ecology of coarse woody debris in temperate ecosystems, *Adv. Ecol. Res.*, *15*, 133–302, 1986.

Harmon, M. E., and J. Sexton, Guidelines for measurements of woody detritus in forest ecosystems, *Publ. 20*, 73 pp., U. S. Long Term Ecol. Res. Network Off., Univ. of Wash., Seattle, 1996.

Heimsath, A. M., W. E. Dietrich, K. Nishiizumi, and R. C. Finkel, The soil production function and landscape equilibrium, *Nature*, *388*, 358–361, 1997.

Heimsath, A. M., W. E. Dietrich, K. Nishiizumi, and R. C. Finkel, Stochastic processes of soil production and transport: Erosion rates, topographic variation, and cosmogenic nuclides in the Oregon Coast Range, *Earth Surf. Processes Landforms*, *26*, 531–552, 2001.

Hogan, D. L., S. A. Bird, and M. A. Hassan, Spatial and temporal evolution of small coastal gravel-bed streams: Influence of forest management on channel morphology and fish habitats, in *Gravel-Bed Rivers in the Environment*, edited by P. C. Klingeman et al., pp. 365–392, Water Resour. Publ., Highlands Ranch, Colo., 1998.

Hough, B. K., *Basic Soils Engineering*, 513 pp., Ronald, New York, 1957.

Huff, M. H., Post-fire succession in the Olympic Mountains, Washington: Forest vegetation, fuels, and avifauna, Ph.D. dissertation, 240 pp., Univ. of Wash., Seattle, 1984.

Tarboton, D. G., R. L. Bras, and I. Rodriguez-Iturbe, On the extraction of channel networks from digital elevation data, *Hydrol. Processes*, *5*, 81–100, 1991.

Torres, R., W. E. Dietrich, D. R. Montgomery, S. P. Anderson, and K. Loague, Unsaturated zone processes and the hydrologic response of a steep, unchanneled catchment, *Water Resour. Res.*, *34*(8), 1865–1879, 1998.

Tucker, G. E., and R. L. Bras, Hillslope processes, drainage density, and landscape morphology, *Water Resour. Res.*, *34*(10), 2751–2764, 1998.

Tucker, G. E., and R. L. Bras, A stochastic approach to modeling the role of climate variability in drainage basin evolution, *Water Resour. Res.*, *36*(7), 1953–1964, 2000.

Tucker, G. E., S. T. Lancaster, N. M. Gasparini, R. L. Bras, and S. M. Rybarczyk, An object-oriented framework for hydrologic and geomorphic modeling using triangulated irregular networks, *Comp. Geosci.*, *27*(8), 959–973, 2001a.

Tucker, G. E., S. T. Lancaster, N. M. Gasparini, and R. L. Bras, The channel-hillslope integrated landscape development (CHILD) model, in *Landscape Erosion and Evolution Modeling*, edited by R. S. Harmon and W. W. Doe III, pp. 349–388, Plenum, New York, 2001b.

Van Sickle, J., and S. V. Gregory, Modeling inputs of large woody debris to streams from falling trees, *Can. J. For. Res.*, *20*(10), 1593–1601, 1990.

Vanoni, V. A., *Sedimentation Engineering*, 745 pp., Am. Soc. of Civ. Eng., Reston, Va., 1975.

Willgoose, G., A statistic for testing the elevation characteristics of landscape simulation models, *J. Geophys. Res.*, *99*(B7), 13,987–13,996, 1994.

Wimberly, M. C., T. A. Spies, C. J. Long, and C. Whitlock, Simulating historical variability in the amount of old forests in the Oregon Coast Range, *Conserv. Biol.*, *14*(1), 167–180, 2000.

Wu, W., and R. C. Sidle, A distributed slope stability model for steep forested basins, *Water Resour. Res.*, *31*(8), 2097–2110, 1995.

———————————

S. K. Hayes and S. T. Lancaster, Department of Geosciences, Oregon State University, 104 Wilkinson Hall, Corvallis, OR 97331-5506, USA. (stephen.lancaster@geo.orst.edu)

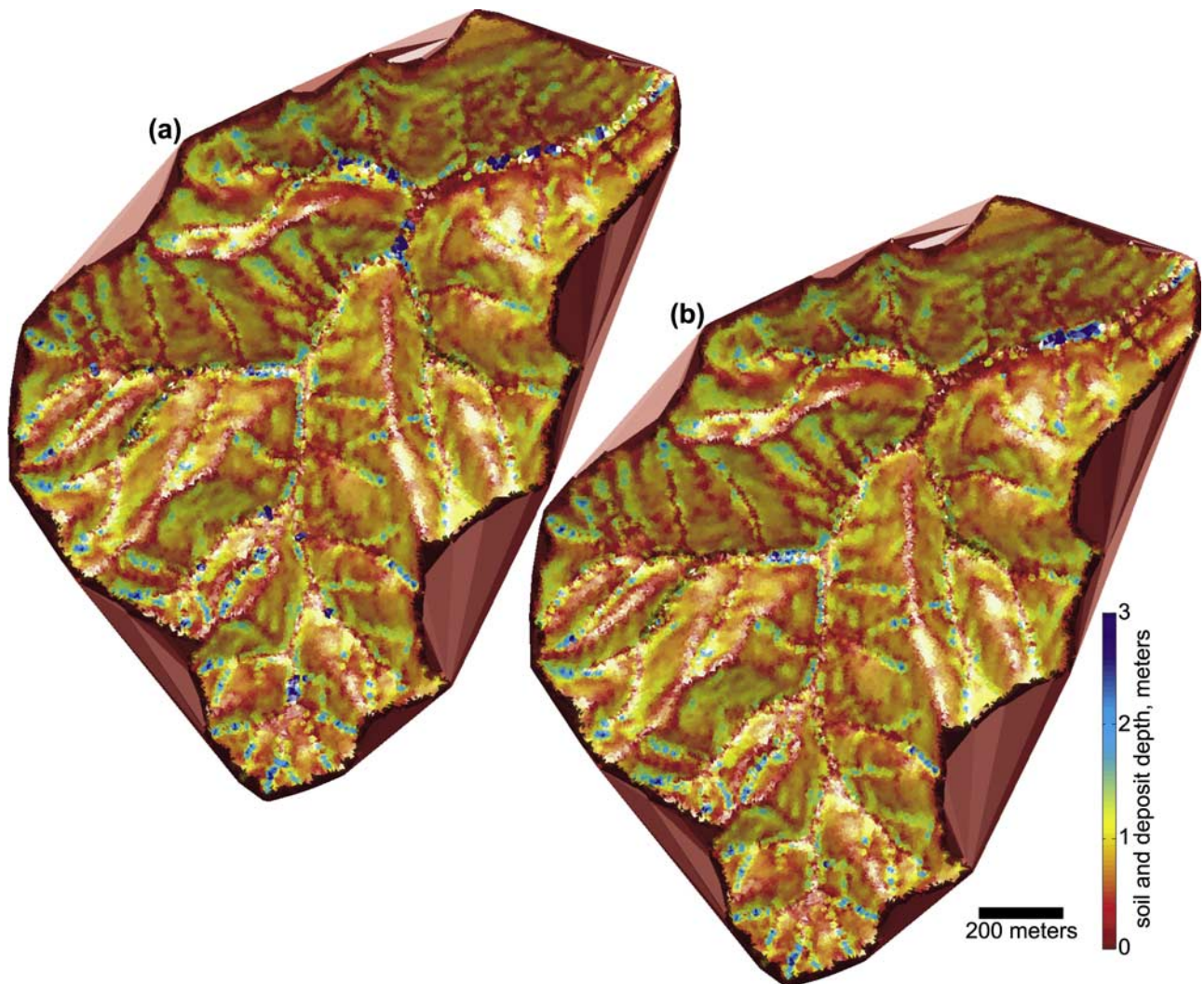G. E. Grant, USDA Forest Service, Pacific Northwest Research Station, Corvallis, OR 97331, USA.

Figure 10. Shaded relief maps colored according to simulated soil, sediment, and wood deposit depth at 200 years (18 years after the fire) for simulation cases (a) with both wood effects (WB) and (b) without either wood effect (NWB). The color scale is compressed to highlight deposits thicker than 3 m, which appear as dark blue patches. Note that the blue channel-side deposits found in both simulations are mainly thick soil accumulations at the bottoms of hillslopes, i.e., remnants of flat valley bottoms that are not affected by the channel-smoothing procedure during initialization.